TKK Radio Science and Engineering Publications

Espoo, June 2008 **REPORT R 3**

ANALYSIS OF ELECTROMAGNETIC SCATTERING FROM ANISOTROPIC IMPEDANCE BOUNDARIES

Thesis for the degree of Doctor of Science in Technology

Ilari Hänninen

Dissertation for the degree of Doctor of Science in Technology to be presented with due permission of the Faculty of Electronics, Communications and Automation, for public examination and debate in Auditorium S 4 at Helsinki University of Technology (Espoo, Finland) on the 6th of June, 2008, at 12 noon.

Helsinki University of Technology
Faculty of Electronics, Communications and Automation
Department of Radio Science and Engineering

Distribution:
Helsinki University of Technology
Department of Radio Science and Engineering
P.O. Box 3000
FI-02015 TKK
Tel. +358 9 451 2261
Fax +358 9 451 2267
E-mail ari.sihvola@tkk.fi

ISBN 978-951-22-9400-8 (printed)
ISBN 978-951-22-9401-5 (electronic)
http://lib.tkk.fi/Diss/2008/isbn9789512294015/
ISSN 1797-4364

Picaset Oy
Helsinki 2008

ABSTRACT OF DOCTORAL DISSERTATION	HELSINKI UNIVERSITY OF TECHNOLOGY P.O. BOX 1000, FI-02015 TKK http://www.tkk.fi

Author Ilari Hänninen

Name of the dissertation
Analysis of electromagnetic scattering from anisotropic impedance boundaries

Manuscript submitted 3.3.2008	Manuscript revised 28.4.2008

Date of the defence 6.6.2008

☐ Monograph ☒ Article dissertation (summary + original articles)

Faculty	Faculty of Electronics, Communications and Automation
Department	Department of Radio Science and Engineering
Field of research	Electromagnetics
Opponent(s)	Professor Tapan Sarkar, Syracuse University, U.S.A.
Supervisor	Professor Keijo Nikoskinen, Professor Jukka Sarvas
Instructor	Professor Keijo Nikoskinen, Professor Jukka Sarvas

Abstract

Analysis of electromagnetic scattering from complex surfaces is an often encountered problem in electrical engineering. Solving such problems is usually difficult, and generally numerical solution methods are needed. Impedance boundary condition (IBC) can often be used to simplify the original scattering problem, if only the fields outside the scatterers are of interest. In this thesis the focus of the research has been on the analysis of scattering from anisotropic impedance surfaces.

The research was divided into two parts. The first part concentrates on the theoretical analysis of scattering using complex boundary conditions. The Perfectly Anisotropic Boundary (PAB) is defined and a possible realization for it is introduced. Similarly, a realization for the the previously introduced Generalized Soft-and-Hard Surface (GSHS) is introduced. The scattering properties of these boundaries are studied, especially regarding the polarization transforming properties.

The second part of the research concentrates on the numerical analysis of scattering from anisotropic impedance boundaries. Surface integral equation formulations for the Soft-and-Hard Surface and a specific IBC surface are presented and the scattering properties of these surfaces are studied. The second part of the research also necessitated the study of the accurate numerical integration techniques, and new results regarding these are given.

In scattering computations the number of unknowns often grows beyond practical limits due to the electrically large size and the complex nature of the studied objects. Thus, more efficient computational methods are needed. The Multilevel Fast Multipole Algorithm (MLFMA) is a very popular such method. In latter part of the thesis a novel and efficient way to compute the translator operator in MLFMA is introduced.

Keywords anisotropic impedance boundary, electromagnetic scattering, surface integral equations

ISBN (printed) 978-951-22-9400-8	ISSN (printed) 1797-4364
ISBN (pdf) 978-951-22-9401-5	ISSN (pdf)
Language English	Number of pages 57 p. + app. 99 p.

Publisher Helsinki University of Technology, Department of Radio Science and Engineering

Print distribution Helsinki University of Technology, Department of Radio Science and Engineering

☒ The dissertation can be read at http://lib.tkk.fi/Diss/2008/isbn9789512294015/

VÄITÖSKIRJAN TIIVISTELMÄ	TEKNILLINEN KORKEAKOULU PL 1000, 02015 TKK http://www.tkk.fi

Tekijä Ilari Hänninen

Väitöskirjan nimi
Sähkömagneettisen sironnan analysointi anisotrooppisista impedanssireunoista

Käsikirjoituksen päivämäärä 3.3.2008	Korjatun käsikirjoituksen päivämäärä 28.4.2008

Väitöstilaisuuden ajankohta 6.6.2008

☐ Monografia	☒ Yhdistelmäväitöskirja (yhteenveto + erillisartikkelit)

Tiedekunta	Elektroniikan, tietoliikenteen ja automaation tiedekunta
Laitos	Radiotieteen ja -tekniikan laitos
Tutkimusala	Sähkömagnetiikka
Vastaväittäjä(t)	Professori Tapan Sarkar, Syracuse University, U.S.A.
Työn valvoja	Professori Keijo Nikoskinen, professori Jukka Sarvas
Työn ohjaaja	Professori Keijo Nikoskinen, professori Jukka Sarvas

Tiivistelmä

Sähkömagneettisen sironnan analysointi monimutkaisista pinnoista on sähkötekniikassa usein eteentuleva ongelma. Tälläisten sirontaongelmien ratkaiseminen on yleensä vaikeaa, ja monesti ratkaisemiseen tarvitaan numeerisia menetelmiä. Impedanssireunaehtoa voidaan usein käyttää yksinkertaistamaan alkuperäistä sirontaongelmaa, jos ainoastaan kentät sirottajien ulkopuolella halutaan ratkaista. Tämän väitöskirjan painopiste on ollut sähkömagneettisen sironnan analysointi anisotrooppisista impendanssireunoista.

Tutkimus jaettiin kahteen osaan. Ensimmäinen osa käsittelee sähkömagneettisen sironnan teoreettista analyysiä käyttäen monimutkaisia reunaehtoja. Täydellinen anisotrooppinen reuna (perfectly anisotropic boundary, PAB) määritellään ja mahdollinen toteutus sille esitellään. Samoin aikaisemmin julkaistulle yleistetylle pehmeä-ja-kova pinnalle (generalized soft-and-hard surface, GSHS) esitellään mahdollinen fysikaalinen toteutus. Näiden reunojen sirontaominaisuuksia tutkitaan, erityisesti polarisaation muuntamisen kannalta.

Tutkimuksen toinen osa käsittelee anisotrooppisten impedanssireunojen sironnan numeerista analyysiä. Pintaintegraaliyhtälöformulaatio sekä pehmeä-ja-kova reunalle että tarkoin määrätylle impedanssireunaehdolle määritellään ja näiden pintojen sirontaominaisuuksia tarkastellaan. Tutkimuksen toinen osa myös teki välttämättömäksi tarkkojen numeeristen integrointitekniikoiden tutkimisen ja näihin liittyen esitellään uusia tuloksia.

Sirontaongelmien laskennassa tuntemattomien muuttujien määrä kasvaa usein käytännöllisten rajojen ulottumattomiin sirottajien suuren sähköisen koon ja monimutkaisen luonteen takia. Tämän takia tehokkaampien laskentamenetelmien tarve on ilmeinen. Nopea monitasoinen multipolialgoritmi (multilevel fast multipole algorithm, MLFMA) on laajalle levinnyt tälläinen menetelmä. Väitöskirjan jälkimmäisessä osassa esitellään uusi ja tehokas tapa laskea nopean monitasoisen multipolialgoritmin translaatiooperaattorin arvoja.

Asiasanat anistrooppinen impedanssireuna, sähkömagneettinen sironta, pintaintegraaliyhtälöt

ISBN (painettu) 978-951-22-9400-8	ISSN (painettu) 1797-4364
ISBN (pdf) 978-951-22-9401-5	ISSN (pdf)
Kieli englanti	Sivumäärä 57 s. + liit. 99 s.

Julkaisija Teknillinen korkeakoulu, radiotieteen ja -tekniikan laitos

Painetun väitöskirjan jakelu Teknillinen korkeakoulu, radiotieteen ja -tekniikan laitos

☒ Luettavissa verkossa osoitteessa http://lib.tkk.fi/Diss/2008/isbn9789512294015/

Acknowledgements

This thesis is based on research work carried out at the Electromagnetics Laboratory of Helsinki University of Technology during the years 2003-2008.

I wish to thank my supervisors Prof. Keijo Nikoskinen and Prof. Jukka Sarvas for their guidance and support. Furthermore, I thank Prof. Ismo Lindell, Prof. Ari Sihvola, Dr. Matti Taskinen for their collaboration.

My sincere thanks also to Docent Pasi Ylä-Oijala and Dr. Seppo Järvenpää for their help. In addition, I thank the rest of the staff of the Electromagnetics Laboratory, and especially Katrina Nykänen for her help with bureaucratic matters.

This research was financially supported by Helsinki University of Technology, Graduate School of Applied Electromagnetics, the Ulla Tuominen Foundation, and the Emil Aaltonen Foundation.

List of Publications

[P1] Ismo V. Lindell, Ari H. Sihvola, and Ilari Hänninen, "Perfectly anisotropic impedance boundary", *IET Microwaves, Antennas & Propagation*, Vol. 1, no. 3, pp. 561-566, 2007.

[P2] Ilari Hänninen, Ismo V. Lindell, and Ari H. Sihvola, "Realization of generalized soft-and-hard boundary", *Progress in Electromagnetics Research*, Vol. 64, pp. 317-333, 2006.

[P3] Ilari Hänninen, Matti Taskinen, and Jukka Sarvas, "Singularity subtraction integral formulae for surface integral equations with RWG, rooftop, and hybrid basis functions", *Progress in Electromagnetics Research*, Vol. 63, pp. 243-278, 2006.

[P4] Ilari Hänninen, Mikko Pitkonen, Keijo I. Nikoskinen, and Jukka Sarvas, "Method of moments analysis of the backscattering properties of a corrugated trihedral corner reflector", *IEEE Transactions on Antennas and Propagation*, Vol. 54, no. 4, pp. 1167-1173, 2006.

[P5] Ilari Hänninen and Keijo Nikoskinen, "Implementation of method of moments for numerical analysis of corrugated surfaces with impedance boundary condition", *IEEE Transactions on Antennas and Propagation*, vol. 56, no. 1, pp. 278-281, 2008.

[P6] Ilari Hänninen and Jukka Sarvas, "Efficient evaluation of the Rokhlin translator in multilevel fast multipole algorithm", *Electromagnetics Laboratory Report Series*, Report 485, Helsinki University of Technology, Espoo, 13 pages, Nov. 2007. Also accepted for publication with minor modifications in *IEEE Transactions on Antennas and Propagation*.

Contribution of the Author

[P1] The paper was the result of a collaboration between the author, Prof. Ismo Lindell, and Prof. Ari Sihvola. Prof. Ismo Lindell was mainly responsible for the manuscript. The author contributed to developing the theory as well as to checking the results.

[P2] The paper was a collaboration between the author, Prof. Ismo Lindell, and Prof. Ari Sihvola. The manuscript was mainly written by the author. In addition, the author was responsible for the numerical computations and for checking the theoretical results.

[P3] The author was mainly responsible for the manuscript, and also derived the analytical results and computed the numerical examples. D.Sc.(Tech) Matti Taskinen provided help with the theoretical aspects of the work, and Prof. Jukka Sarvas gave fruitful comments on the manuscript during the preparation.

[P4] The author was mainly responsible for the paper. The author wrote the computer codes and computed the numerical results presented in the paper, and wrote the manuscript. Mikko Pitkonen provided the Physical Optics results for verification. Prof. Keijo Nikoskinen provided insight with physical aspects of the problem and help with the manuscript, and Prof. Jukka Sarvas helped with the numerical algorithms and gave comments on the manuscript during the preparation.

[P5] The author was mainly responsible for the paper. The original idea behind the paper was the result of discussions between the author and Prof. Keijo Nikoskinen. The author wrote the computer codes and computed the numerical results for the paper. Prof. Keijo Nikoskinen gave comments on the manuscript during the preparation.

[P6] The author was mainly responsible for the paper, with the manuscript written in collaboration by the author and Prof. Jukka Sarvas. The author was also responsible for the numerical computations and the results presented in the paper.

List of Symbols and Abbreviations

$\boldsymbol{a}$ vector

$\hat{\boldsymbol{a}}(=\boldsymbol{a}/|\boldsymbol{a}|)$ unit vector

$\boldsymbol{ab}$ dyad

$\overline{\overline{\mathsf{A}}}$ dyadic (a polynomial of dyads)

$\boldsymbol{E}$ electric field

$\boldsymbol{H}$ magnetic field

$\boldsymbol{D}$ electric flux density

$\boldsymbol{B}$ magnetic flux density

$\boldsymbol{J}$ electric current density

$\boldsymbol{M}$ magnetic current density

ρ electric charge density

ρ_m magnetic charge density

ϵ electric permittivity

μ magnetic permeability

ω angular frequency

k wave number

$\mathcal{L}$ linear (integral) operator

$\mathcal{O}(f(n))$ proportional to the function $f(n)$

IBC Impedance Boundary Condition

PEMC Perfect Electric and Magnetic Conductor

PAB Perfectly Anisotropic Boundary

SHS Soft-and-Hard Surface

GSHS Generalized Soft-and-Hard Surface

MoM Method of Moments

FMM Fast Multipole Method

MLFMA Multilevel Fast Multipole Algorithm

Contents

1 Introduction

Modeling of electromagnetic scattering from various objects is a commonly encountered problem in electrical engineering. If the scattering problem involves multiple scatterers which are penetrable by electromagnetic fields, then the fields must be solved in multiple regions inside and outside the scatterers. The more numerous and the more varied in their electrical properties the scatterers are, the more difficult the solving of the scattering problem becomes.

Even for a single object finding a solution for the scattering problem may be very difficult, if the surface structure of the scatterer is sufficiently complicated. Such surfaces that are often encountered in scattering problems are, for example, corrugated surfaces of various cross-sectional shapes, fractal surfaces, planar antenna structures, composite material mixtures, many meta-material realizations, etc. (see Fig. 1).

If the fields only outside the scatterer are of interest, then a great number of scattering problems would be greatly simplified if, instead of using the original complicated surface structure, the presence of the scatterer could be simulated by a boundary condition. Then the scattering problem would only involve a smoother and simpler surface, thus providing a more efficient numerical solution.

However, a boundary condition is a mathematical idealization of a complex situation, and finding a suitable one for the given problem is not a trivial task. Many factors must be taken into account if one wishes to make such an approximation: the curvature of the original scatterer, the penetration depth, the nature and the direction of the incident field, etc. Fortunately, for many kinds of surfaces there exists an impedance boundary condition that is a sufficiently accurate idealization. But finding a well fitting boundary condition is usually only the first step on the path to solve the studied problem.

As the solving of a complicated scattering problem usually involves some sort of numerical solution method, this introduces a new set of problems. Implementing an accurate numerical method for solving a scattering problem with a specific boundary condition is often not a straightforward process. Surface integral equation methods are often used in solving electromagnetic scattering problems, but finding an efficient and accurate formulation for a given problem may be difficult. Also, numerical integration methods, despite having been carefully studied since the birth of scientific computing, remain still a problematic area.

There are also situations when the analysis of the scattering from a surface defined by a boundary condition is not of primary interest. Instead, the goal may be to find or to synthesize a material or a meta-material that

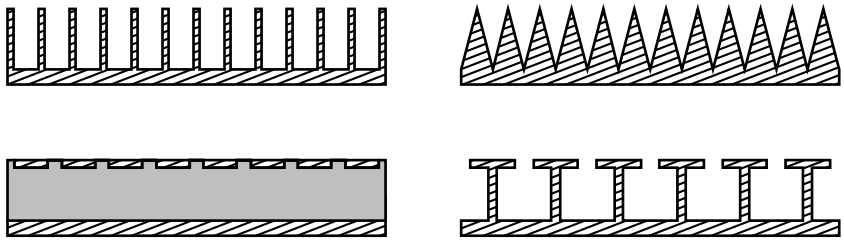

Figure 1: Different types of complex surfaces

corresponds to a specific kind of a boundary condition. These situations may arise, for example, when trying to realize certain specific scattering characteristics for an antenna, and a suitable boundary condition would satisfy these requirements.

In this thesis the focus of the research has been the analysis of the electromagnetic scattering from anisotropic impedance surfaces, i.e. surfaces that have some preferred direction for the electric and magnetic fields. The goal was to develop new analytical and numerical methods for scattering analysis. The research was branched into two problem areas.

The first area was the theoretical analysis of the scattering properties of complex anisotropic boundary conditions, and also the study of their possible realizations. The second problem area was the numerical analysis of scattering from surfaces that can be approximated by anisotropic boundary conditions. In addition to studying the numerical methods, the second part of the research also led to the development of some new results for the numerical integration techniques involved.

However, it is not sufficient to propose a numerical solution method for a problem without verifying its accuracy. Also, when finding possible realizations for complex boundary conditions it must be carefully verified that the synthesized material exactly produces the desired boundary condition and the scattering behavior. This means in many cases that the full, accurate model of the original complex surface structure must be studied. This may prove to be problematic as the surface may have many electrically small details, so that the accurate modeling would require impracticable computational resources.

During recent years, there has been a considerable interest in the Multilevel Fast Multipole Algorithm (MLFMA), which has been successfully used to solve very large scattering problems. MLFMA can be used in many cases to verify that the impedance boundary approximations accurately model the scattering behavior of the original object. MLFMA can

also be used in conjunction with complex boundary condition to further increase the size of the studied problems by making the most efficient use of the available computational resources. For these reasons, the last part of the research concentrated on the MLFMA.

2 Anisotropic Impedance Boundary

An impedance boundary condition (IBC) defines a relationship between the time-harmonic tangential electric and magnetic fields on a surface. To study this relationship between the fields, one must start by studying the Maxwell equations.

The Maxwell equations in the frequency domain are (with a suppressed time factor $e^{-i\omega t}$)

$$\nabla \times \boldsymbol{E} = i\omega \boldsymbol{B}, \tag{1}$$

$$\nabla \times \boldsymbol{H} = -i\omega \boldsymbol{D} + \boldsymbol{J}, \tag{2}$$

$$\nabla \cdot \boldsymbol{B} = 0, \tag{3}$$

$$\nabla \cdot \boldsymbol{D} = \rho. \tag{4}$$

Often, for symmetry reasons, the magnetic current density $\boldsymbol{M}$ is introduced into the equation (1),

$$\nabla \times \boldsymbol{E} = i\omega \boldsymbol{B} - \boldsymbol{M}, \tag{5}$$

and similarly, the magnetic charge density ρ_m is introduced into the equation (3),

$$\nabla \cdot \boldsymbol{B} = \rho_m. \tag{6}$$

The Maxwell equations (1)-(4) contain two vector and two scalar equations and four vector unknowns. To guarantee a unique solution for the fields, the medium equations (i.e. the constitutive relations) must also be introduced. They can be written in the general form [43]

$$\boldsymbol{D} = \overline{\overline{\epsilon}} \cdot \boldsymbol{E} + \overline{\overline{\xi}} \cdot \boldsymbol{H}, \tag{7}$$

$$\boldsymbol{B} = \overline{\overline{\zeta}} \cdot \boldsymbol{E} + \overline{\overline{\mu}} \cdot \boldsymbol{H}. \tag{8}$$

For a linear medium the dyadic medium parameters $\overline{\overline{\epsilon}}$, $\overline{\overline{\xi}}$, $\overline{\overline{\zeta}}$, $\overline{\overline{\mu}}$ depend on the electric and magnetic properties of the medium. The medium parameters mask all the physical phenomena of the medium, so that the macroscopic electromagnetic fields behave similarly for two different media with the same medium parameters even though the media in question may have significantly different physical characteristics.

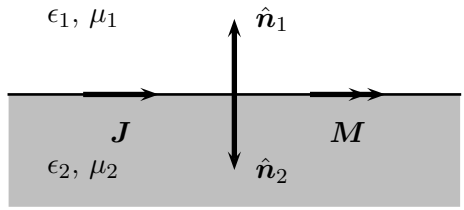

Figure 2: Interface between two media.

The Maxwell equations in their differential form are not valid everywhere if the medium parameters are discontinuous, since some of the field components may then also be discontinuous and thus their derivatives would be infinite. Unfortunately, one often encounters such situations in electromagnetic computations, e.g. a model may contain two different materials that have different medium parameters. In such a case, the interface conditions relate the discontinuous fields to the discontinuous sources, and they are written as

$$\hat{\boldsymbol{n}}_1 \times \boldsymbol{E}_1 + \hat{\boldsymbol{n}}_2 \times \boldsymbol{E}_2 = -\boldsymbol{M}, \tag{9}$$

$$\hat{\boldsymbol{n}}_1 \times \boldsymbol{H}_1 + \hat{\boldsymbol{n}}_2 \times \boldsymbol{H}_2 = \boldsymbol{J}, \tag{10}$$

where $\boldsymbol{E}_1$ and $\boldsymbol{H}_1$ are the electric field and the magnetic field in the volume V_1 with medium coefficients ϵ_1, μ_1, the unit normal vector $\hat{\boldsymbol{n}}_1$ on the interface pointing to the volume V_1, and similarly for the subscript $()_2$ for the volume V_2 (see Fig. 2). $\boldsymbol{J}$ and $\boldsymbol{M}$ are the electric and magnetic current sources at the interface.

If the interface is a closed surface S that completely bounds the volume V_2, it may be possible to significantly simplify the original scattering problem. The Huygens' equivalence principle defines the so-called equivalent surface currents on the surface S which create fields outside of V_2 that exactly cancel the fields produced by the original sources in V_2 [45] (see Fig. 3). Thus, these equivalent surface currents produce exactly the same fields outside V_2 as the original sources.

The equivalent surface currents can be obtained from the interface conditions (9), (10) by requiring that the fields $\boldsymbol{E}_2$ and $\boldsymbol{H}_2$ vanish outside V_2, in which case one can write

$$\boldsymbol{J} = \hat{\boldsymbol{n}} \times \boldsymbol{H}, \tag{11}$$

$$\boldsymbol{M} = -\hat{\boldsymbol{n}} \times \boldsymbol{E}, \tag{12}$$

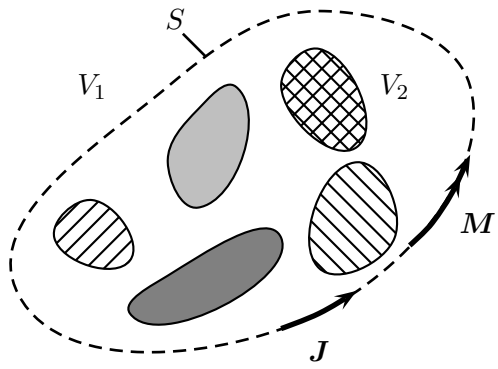

Figure 3: Using the Huygens' equivalence principle and equivalent surface currents, the original scattering problem may be reduced to a simpler one.

for fields on the boundary, with $\hat{\boldsymbol{n}}$ pointing away from the region V_2. By enveloping the original scatterer by the surface S and using the equivalent surface currents (11) and (12) as sources, it is possible to replace the original scattering problem by a new one.

2.1 Different Kinds of Boundary Conditions

The use of Huygens' equivalence principle to simplify the original scattering problem introduces a new problem: What kind of a boundary condition on the surface S models accurately the scattering behavior of the original scatterers? Usually, the equivalent current sources on Huygens' boundary are unknown (as are the original induced sources), so some physical insight and knowledge of the original scatterers must be used to shed light on the problem.

The impedance boundary condition (IBC) defines a linear relation between the the tangential electric field $\boldsymbol{E}_t$ and the tangential magnetic field $\boldsymbol{H}_t$ in the interface conditions (11), (12). The impedance boundary condition is generally an approximation of the real interface conditions, although there are situations where it can be considered to be exact. If the error made in the approximation is sufficiently small, then it is usually safe to use the IBC in numerical solution procedures. Typically, a medium with a large refractive index can be handled through IBC.

The IBC can be written in the following equivalent forms [43],

$$\boldsymbol{E}_t = -\overline{\overline{\mathsf{Z}}}_s \cdot \hat{\boldsymbol{n}} \times \boldsymbol{H}, \quad -\hat{\boldsymbol{n}} \times \boldsymbol{H} = \overline{\overline{\mathsf{Y}}}_s \cdot \boldsymbol{E}_t, \tag{13}$$

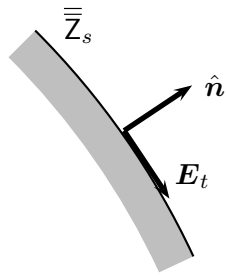

Figure 4: Impedance boundary.

where $\overline{\overline{\mathsf{Z}}}_s$ is the surface impedance dyadic, $\overline{\overline{\mathsf{Y}}}_s = \overline{\overline{\mathsf{Z}}}_s^{-1}$ is the surface admittance dyadic, and $\hat{\boldsymbol{n}}$ is the outward directed unit normal vector to the surface S (see Fig. 4). The surface impedance and admittance dyadics satisfy

$$\hat{\boldsymbol{n}} \cdot \overline{\overline{\mathsf{Z}}}_s = \overline{\overline{\mathsf{Z}}}_s \cdot \hat{\boldsymbol{n}} = 0, \quad \hat{\boldsymbol{n}} \cdot \overline{\overline{\mathsf{Y}}}_s = \overline{\overline{\mathsf{Y}}}_s \cdot \hat{\boldsymbol{n}} = 0. \tag{14}$$

The simplest form of an impedance boundary is the isotropic boundary, which is defined to have an impedance dyadic of the form

$$\overline{\overline{\mathsf{Z}}}_s = Z_s \bar{\bar{\mathsf{I}}}_t, \quad \overline{\overline{\mathsf{Y}}}_s = Y_s \bar{\bar{\mathsf{I}}}_t, \tag{15}$$

where $\bar{\bar{\mathsf{I}}}_t = \hat{\boldsymbol{u}}\hat{\boldsymbol{u}} + \hat{\boldsymbol{v}}\hat{\boldsymbol{v}}$ is the unit dyadic tangential to the surface, and $Y_s = 1/Z_s$. The unit vectors $\hat{\boldsymbol{u}}$ and $\hat{\boldsymbol{v}}$ are local orthogonal tangential vectors on the surface, so that $\hat{\boldsymbol{u}} \times \hat{\boldsymbol{v}} = \hat{\boldsymbol{n}}$.

A special case of an isotropic impedance boundary is the Perfect Electric Conductor (PEC) boundary that is often applied as an approximation for materials made of good electric conductors. The PEC boundary condition can be obtained from (12) by setting $\boldsymbol{M} = 0$,

$$\hat{\boldsymbol{n}} \times \boldsymbol{E} = 0. \tag{16}$$

The PEC boundary condition assumes that the conductivity of the material is infinite, so the corresponding impedance dyadic is $\overline{\overline{\mathsf{Z}}}_s = 0$. Analogously one can also define the Perfect Magnetic Conductor (PMC) boundary condition for magnetic fields from (11) by setting $\boldsymbol{J} = 0$,

$$\hat{\boldsymbol{n}} \times \boldsymbol{H} = 0. \tag{17}$$

Similarly as in the case of the PEC boundary, the admittance dyadic for the PMC surface is $\overline{\overline{\mathsf{Y}}}_s = 0$.

The PEC and the PMC boundary conditions can be combined to form the Perfect Electric and Magnetic Conductor (PEMC) boundary condition [46],

$$\hat{\boldsymbol{n}} \times (\boldsymbol{H} + M\boldsymbol{E}) = 0, \tag{18}$$

where M denotes the admittance of the PEMC boundary. The PMC boundary condition corresponds to the case $M = 0$ and the PEC boundary condition can be obtained as the limit $M \to \infty$.

The isotropic boundary can also be considered a special case of the more general bi-isotropic boundary that has an impedance dyadic of the following form,

$$\overline{\overline{\mathsf{Z}}}_s = Z_a \overline{\mathsf{I}}_t + Z_b \overline{\mathsf{J}}, \tag{19}$$

with $\overline{\mathsf{J}} = \hat{\boldsymbol{n}} \times \overline{\mathsf{I}}_t$. The unit dyadic $\overline{\mathsf{I}}_t$ and the antisymmetric dyadic $\overline{\mathsf{J}}$ are isotropic, since they do not depend on the choice of the vector basis. Any impedance boundary is called isotropic if its impedance or admittance dyadic can be expressed in terms of isotropic dyadics. Neither the isotropic nor the bi-isotropic boundaries have any preferred direction in the tangent plane of the surface.

If the impedance depends on the direction of the fields, the surface is called anisotropic. In the simplest form the anisotropic impedance dyadic can be written

$$\overline{\overline{\mathsf{Z}}}_s = Z_u \hat{\boldsymbol{u}}\hat{\boldsymbol{u}} + Z_v \hat{\boldsymbol{v}}\hat{\boldsymbol{v}}, \quad \overline{\overline{\mathsf{Y}}}_s = Y_u \hat{\boldsymbol{u}}\hat{\boldsymbol{u}} + Y_v \hat{\boldsymbol{v}}\hat{\boldsymbol{v}}, \tag{20}$$

where $Y_u = 1/Z_u$, $Y_v = 1/Z_v$, so that the impedance is Z_u for tangential electric field polarized along $\hat{\boldsymbol{u}}$ and, correspondingly, Z_v for the tangential field along $\hat{\boldsymbol{v}}$.

In general, a planar anisotropic dyadic can be written as a linear combination of the dyadics $\overline{\mathsf{I}}_t$, $\overline{\overline{\mathsf{J}}}$, and

$$\overline{\overline{\mathsf{K}}} = \hat{\boldsymbol{u}}\hat{\boldsymbol{u}} - \hat{\boldsymbol{v}}\hat{\boldsymbol{v}}, \quad \overline{\overline{\mathsf{L}}} = \hat{\boldsymbol{u}}\hat{\boldsymbol{v}} + \hat{\boldsymbol{v}}\hat{\boldsymbol{u}}, \tag{21}$$

as shown in [P1]. As opposed to the isotropic dyadics $\overline{\mathsf{I}}_t$ and $\overline{\overline{\mathsf{J}}}$ the dyadics $\overline{\overline{\mathsf{K}}}$ and $\overline{\overline{\mathsf{L}}}$ depend on the chosen basis vectors. In [P1], the so-called Perfectly Anisotropic Boundary (PAB) was defined as having a surface impedance dyadic that can be expressed only in terms of $\overline{\overline{\mathsf{K}}}$ and $\overline{\overline{\mathsf{L}}}$, i.e. in the form

$$\overline{\overline{\mathsf{Z}}} = Z_c \overline{\overline{\mathsf{K}}} + Z_d \overline{\overline{\mathsf{L}}}. \tag{22}$$

A special case of the anisotropic impedance boundary is called the Soft-and-Hard Surface (SHS) boundary, for which the boundary condition can be written in the form [33, 34]

$$\hat{\boldsymbol{u}} \cdot \boldsymbol{E} = 0, \quad \hat{\boldsymbol{u}} \cdot \boldsymbol{H} = 0. \tag{23}$$

The anisotropic impedance dyadic for the SHS is obtained from (20) with $Z_u = 0$, and as the limit $Z_v \to \infty$. The SHS behaves as a PEC surface for tangential electric fields $\boldsymbol{E}_t$ parallel to $\hat{\boldsymbol{u}}$, whereas for tangential magnetic fields $\boldsymbol{H}_t$ parallel to $\hat{\boldsymbol{u}}$ it behaves as a PMC surface.

A more general class of soft-and-hard boundaries can be defined by the condition [44]

$$\boldsymbol{a} \cdot \boldsymbol{E} = 0, \quad \boldsymbol{b} \cdot \boldsymbol{H} = 0, \tag{24}$$

where $\boldsymbol{a}$ and $\boldsymbol{b}$ are complex vectors satisfying the conditions $\hat{\boldsymbol{n}} \cdot \boldsymbol{a} = 0$, $\hat{\boldsymbol{n}} \cdot \boldsymbol{b} = 0$, and

$$\boldsymbol{a} \cdot \boldsymbol{b} = 1. \tag{25}$$

The boundary condition (24) defines the so-called Generalized Soft-and-Hard Surface (GSHS).

2.2 Realization of an Impedance Boundary

Finding a realization for a given boundary condition and the corresponding surface impedance dyadic is not a trivial task. Often there are several different ways in which a boundary condition can be realized. As the material parameters $\overline{\overline{\epsilon}}$, $\overline{\overline{\mu}}$, $\overline{\overline{\xi}}$, and $\overline{\overline{\zeta}}$ are related to the boundary condition through the interface conditions, finding the expressions for the medium dyadics is often the first step in the process of finding a possible realization for the boundary condition.

If the material behaves similarly in all directions, i.e. it has no special directions, then it is called isotropic or bi-isotropic. As an example, the PEC surface is often used as an approximation for metal structures, i.e. good electric conductors. For such materials the penetration depth of and the dependency on the angle of incidence of the electric field inside the material are very small, so in practice the PEC boundary condition can be used for these types of materials without much concern as the error made in the impedance boundary approximation is small. Similarly, the PMC boundary condition can be used in situations where the magnetic field does not depend on the incident angle nor on the penetration depth of the magnetic field into the material.

Generally speaking, an isotropic surface impedance of the form $\overline{\overline{\mathsf{Z}}} = Z\overline{\overline{\mathsf{I}}}_t$ can be obtained by a slab of isotropic material with $\overline{\overline{\epsilon}} = \epsilon\overline{\overline{\mathsf{I}}}_t$, $\overline{\overline{\mu}} = \mu\overline{\overline{\mathsf{I}}}_t$. If the surface impedance dyadic is bi-isotropic, i.e. it has a component of the form $Z\overline{\overline{\mathsf{J}}}$, then the surface impedance may be realized by a gyrotropic material. The PEMC boundary condition (18) is an example of such a surface, and a planar PEMC surface can be realized with a gyrotropic slab backed by a PEC plate, with the gyrotropic medium defined by the

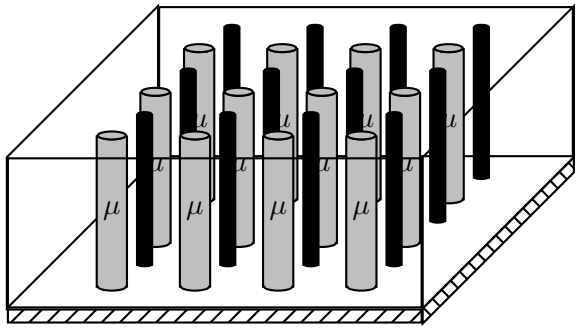

Figure 5: Possible realizations for PAB and GSHS surfaces are based on high-permeability rods and metal wires embedded in a dielectric slab backed by a PEC plane.

medium dyadics [47]

$$\bar{\bar{\epsilon}} = \epsilon \left(\bar{\bar{\mathsf{I}}}_t + ie\bar{\bar{\mathsf{J}}} + e_z \hat{\boldsymbol{n}}\hat{\boldsymbol{n}} \right), \quad \bar{\bar{\mu}} = \mu \left(\bar{\bar{\mathsf{I}}}_t + im\bar{\bar{\mathsf{J}}} + m_z \hat{\boldsymbol{n}}\hat{\boldsymbol{n}} \right), \tag{26}$$

where e, e_z, m, and m_z are dimensionless parameters.

For a PAB surface, if it is assumed that the surface admittance dyadic is of the form (see [P1])

$$\bar{\bar{\mathsf{Y}}} = iB_s \bar{\bar{\mathsf{K}}}, \tag{27}$$

where B_s is a real surface susceptance, the medium dyadics can both be assumed to be multiples of $\bar{\bar{\mathsf{K}}}$, i.e.

$$\bar{\bar{\epsilon}}_t = \epsilon_k \bar{\bar{\mathsf{K}}}, \quad \bar{\bar{\mu}}_t = \mu_k \bar{\bar{\mathsf{K}}}. \tag{28}$$

Similarly, in [P2] it was shown that for a GSHS, the medium dyadics required for its realization may be written in the following form,

$$\bar{\bar{\epsilon}}_t = \frac{1}{k_0 d} \left(\pi^2 A \boldsymbol{ab} - B \boldsymbol{ab}^{\times}_{\times} \hat{\boldsymbol{n}}\hat{\boldsymbol{n}} \right) \tag{29}$$

$$\bar{\bar{\mu}}_t = \frac{1}{k_0 d} \left(-\frac{\pi^2}{4B} \boldsymbol{ab} + \frac{1}{A} \boldsymbol{ab}^{\times}_{\times} \hat{\boldsymbol{n}}\hat{\boldsymbol{n}} \right) \tag{30}$$

where the parameters A and B depend on the practical realization. (In the equations (29) and (30) the double cross product for two dyads $\boldsymbol{ab}$ and $\boldsymbol{cd}$ is defined as $\boldsymbol{ab}^{\times}_{\times}\boldsymbol{cd} = (\boldsymbol{a} \times \boldsymbol{c})(\boldsymbol{b} \times \boldsymbol{d})$ [43].) In [P1] and [P2] possible realizations for the PAB and GSHS surfaces are given based on the work

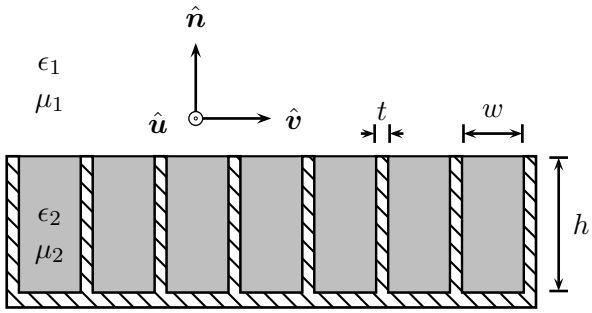

Figure 6: Side profile of the corrugation.

by Prof. I. Lindell and Prof. A. Sihvola [48]. These realizations include high-permeability rods and metallic wires embedded in a dielectric slab backed by a PEC plate (see Fig. 5).

The SHS boundary is of particular interest for scattering computations, since it has many applications in antenna engineering and it can be realized in simple ways, for example, by using thin parallel wires above a PEC plate, or by a corrugated surface. To realize an SHS boundary, an impedance boundary of the form (20) with $Z_u = 0$, $Z_v \to \infty$ is required.

This kind of a surface can be realized by a corrugated plate with the grooves of the corrugation filled with a dielectric material depicted in the Fig. 6. The grooves of the corrugation can be approximated by short-circuited waveguides. If the width w of the grooves of the corrugation is sufficiently small, i.e. $w \ll \lambda$, where λ is the wavelength of the incident wave, and the thickness t of the walls between the grooves is much smaller than the width, $t \ll w$, then the corrugated surface can be approximated by an impedance boundary.

If the incident electric field is in the plane formed by the surface normal $\hat{\boldsymbol{n}}$ and the vector $\hat{\boldsymbol{u}}$, the dominant waveform created inside the grooves is the evanescent TE_1 mode [8], and the surface impedance seen by the incident electric field is

$$Z_u = iZ^{\mathrm{TE}_1} \tan\left(\beta^{\mathrm{TE}_1} h\right), \tag{31}$$

where $Z^{\mathrm{TE}_1} = \omega\mu_2/\beta^{\mathrm{TE}_1}$ is the wave impedance for the TE_1-waveform, β^{TE_1} is the propagation factor, and μ_2 is the permeability inside the corrugation. For incident electric field in the plane formed by the surface normal $\hat{\boldsymbol{n}}$ and the vector $\hat{\boldsymbol{v}}$, the waveform created inside the grooves is a

standing TEM wave, and the surface impedance is given by

$$Z_v = i\eta_2 \tan(k_{2n}h), \tag{32}$$

where $k_{2n} = |\hat{\boldsymbol{n}} \cdot \boldsymbol{k}_2|$, and $\eta_2 = \sqrt{\frac{\mu_2}{\epsilon_2}}$ is the wave impedance inside the corrugation.

If the groove height h of the corrugation is also chosen properly, i.e. if the groove height is tuned to the incident frequency, then the corrugated surface can be made to approximate the SHS. The resonant height of the corrugation is

$$h_r = \frac{\lambda}{4\sqrt{\epsilon_2/\epsilon_1 - \sin^2\alpha}}, \tag{33}$$

where α is the incident angle measured from the surface normal towards the $\hat{\boldsymbol{u}}$-direction, and ϵ_1 and ϵ_2 are the permittivities outside and inside the grooves, respectively. With the height of the corrugation chosen as in (33), the following limits for the impedance components apply,

$$\lim_{w\to 0} Z_u = 0, \quad \lim_{h\to h_r} Z_v = \infty. \tag{34}$$

2.3 Applications of Anisotropic Boundaries

Impedance boundary conditions are often used as approximations for modeling the macroscopic behavior of complicated surface structures in electromagnetic scattering [27, 60, 61, 73]. More specifically, corrugations and SHSs also have been used in many applications, e.g. in radar calibration, remote sensing, antenna and waveguide engineering [19, 35, 49, 50, 62].

One of the the main properties of anisotropic boundaries is polarization transformation of reflected fields, which can be exploited for example in antenna and waveguide applications. In [P1] and [P2] this property of the PAB and the GSHS surfaces is studied analytically. Similarly in [P4] and [P5] electromagnetic scattering from corrugated structures is numerically examined. The methods and the results of [P4] and [P5] are introduced in the Section 4.

The polarization transformation can be studied analytically by means of Geometrical Optics (GO) and the reflection dyadic $\overline{\overline{\mathsf{R}}}$. Using the reflection dyadic one can write the reflected field from a surface as

$$\boldsymbol{E}^r = \overline{\overline{\mathsf{R}}} \cdot \boldsymbol{E}^i, \tag{35}$$

where $\boldsymbol{E}^i$ is the incident field. Generally, the reflection dyadic depends on the propagation direction of the incident field, thus $\overline{\overline{\mathsf{R}}} = \overline{\overline{\mathsf{R}}}(\boldsymbol{E}^i)$ and (35) is not a linear relation.

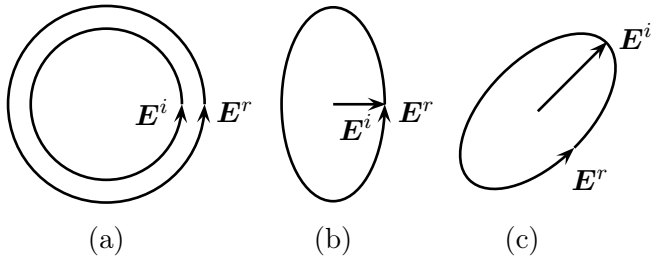

Figure 7: Reflection of a circularly polarized field from (a) an SHS retains the original handedness; reflections from (b) GSHS and (c) PAB surfaces can transform a linearly polarized incident filed into an elliptically polarized field.

If the incidence is restricted to the normal direction, then for the planar GSHS defined on the xy-plane by the vectors

$$\begin{aligned} \boldsymbol{a} &= \hat{\boldsymbol{x}} \cos\varphi + i\hat{\boldsymbol{y}} \sin\varphi, \\ \boldsymbol{b} &= \hat{\boldsymbol{x}} \cos\varphi - i\hat{\boldsymbol{y}} \sin\varphi = \boldsymbol{a}^*. \end{aligned} \tag{36}$$

the reflection dyadic can be written (see [P2])

$$\overline{\overline{\mathsf{R}}} = -\overline{\overline{\mathsf{K}}} \cos 2\varphi + i\overline{\overline{\mathsf{J}}} \sin 2\varphi. \tag{37}$$

For a regular SHS surface, which can be obtained from (36) by setting $\varphi = 0$, the reflection dyadic is simply

$$\overline{\overline{\mathsf{R}}} = -\overline{\overline{\mathsf{K}}}. \tag{38}$$

Similarly, for a planar PAB defined by (27), the reflection dyadic can be written and for normal incidence (see [P1])

$$\overline{\overline{\mathsf{R}}} = \bar{\bar{\mathsf{I}}}_t \cos 2\psi - i\overline{\overline{\mathsf{K}}} \sin 2\psi, \tag{39}$$

where

$$\tan\psi = \eta_0 B_s. \tag{40}$$

Using the above reflection dyadics and a circularly polarized incident wave $\boldsymbol{E}^i = E_0(\hat{\boldsymbol{u}} + i\hat{\boldsymbol{v}})$ to compute the reflected field, we can easily see that the field reflected from an SHS retains the original handedness,

$$\boldsymbol{E}^r = -E_0 \overline{\overline{\mathsf{K}}} \cdot (\hat{\boldsymbol{u}} + i\hat{\boldsymbol{v}}) = E_0(\hat{\boldsymbol{u}} - i\hat{\boldsymbol{v}}). \tag{41}$$

For the GSHS defined by (36) and for a linearly polarized incident field $\boldsymbol{E}^i = E_0\hat{\boldsymbol{u}}$, the reflected field is elliptically polarized,

$$\boldsymbol{E}^r = E_0(-\overline{\overline{\mathsf{K}}}\cos 2\varphi + i\overline{\overline{\mathsf{J}}}\sin 2\varphi)\cdot\hat{\boldsymbol{u}} = -E_0(\cos 2\varphi\hat{\boldsymbol{u}} - i\sin 2\varphi\hat{\boldsymbol{v}}), \quad (42)$$

with the ellipticity of the reflected field determined by the parameter φ. Similarly, for a PAB surface and for a linearly polarized incident field $E^i = E_0(\hat{\boldsymbol{u}} + \hat{\boldsymbol{v}})$, the reflected field $\boldsymbol{E}^r$ is elliptically polarized,

$$\boldsymbol{E}^r = \cos 2\psi(\hat{\boldsymbol{u}} + \hat{\boldsymbol{v}}) - i\sin 2\psi(\hat{\boldsymbol{u}} - \hat{\boldsymbol{v}}), \quad (43)$$

with the ellipticity determined by the value of the parameter ψ. (See Fig. 7 for these examples.)

3 Numerical Methods

When solving difficult scattering problems, especially those involving complicated boundary structures or conditions, one must often resort to computational methods. The field of computational electromagnetics has been studied extensively during the last decades and the literature covering the different methods is vast [3, 31, 41, 51, 53, 57, 68]. The techniques used in the analysis of electromagnetic scattering can be broadly divided into methods based on differential equations and integral equations.

On the differential equation side the most commonly used methods are the Finite-Difference Time-Domain (FD-TD) method [42, 69, 81] and the Finite Element Method (FEM) [30, 52, 58, 63, 76]. In these methods the whole computational domain is discretized and the fields are the unknowns to be solved for. The advantages of these methods are that the resulting system matrix in the FEM is sparse (or, as is in the case of FD-TD, there is no actual system matrix).

On the other hand, for scattering problems or other such problems that involve an unbounded domain, the system matrix needs to be computed for the whole computational domain, which leads to a large number of unknowns. Naturally, the computational domain must be artificially limited, e.g. using absorbing boundary conditions or Perfectly Matched Layers (PMLs) [1], which adds a dimension of complexity to formulating these methods.

When using integral equation based methods, such as the Method of Moments (MoM) [25, 79], equivalent sources are used as unknowns instead of the fields. This means that the resulting system matrix is usually a full matrix, and its elements are computed from singular integrals. The advantage of these methods is that the number of unknowns, especially

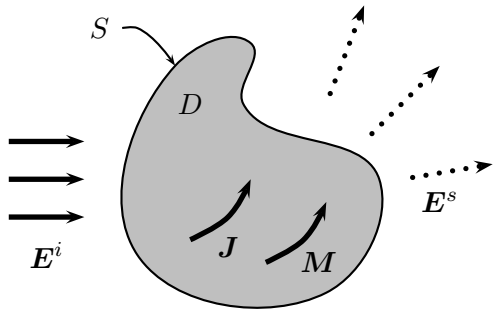

Figure 8: Using the equivalent surface current sources $\boldsymbol{J}$ and $\boldsymbol{M}$ on the surface S of the scatterer D, the scattering problem can be simplified.

for surface integral equations, is usually much smaller than for the corresponding differential equation based solution. Surface integral equations based methods are also well suited for scattering and radiation problems that involve unbounded domains.

The disadvantages of integral equation based methods include the difficulties involved in the numerical integration of the singular kernels and inverting the full system matrix. The former problem has been the subject of extensive research and is studied in the paper [P3]. To alleviate the latter problem, iterative solution methods may be used instead of direct matrix inversion.

However, the use of iterative solution methods only somewhat speeds up the computations. The computational cost of the full matrix inversion is $\mathcal{O}(N^3)$, for N unknowns, while the iterative solvers typically have a computational cost of $\mathcal{O}(N^2)$. However, for large problems, even when using iterative solution methods, the required computational costs often exceed the available resources.

Fast solvers, e.g. FFT-based methods, the adaptive integral equation method and the Fast Multipole Method (FMM), are often used to speed up the computations when the number of unknowns grows beyond the limit that a straight-forward integral equation based solution method can handle. The FMM is discussed in more detail in Section 5.

3.1 Surface Integral Equations for Scattering Problems

Consider the scattering problem presented in the Fig. 8, where $\boldsymbol{E}^i$ and $\boldsymbol{E}^s$ are the incident (primary) field and the scattered field, respectively.

The medium outside the scatterer D is assumed to be homogeneous and isotropic material or vacuum.

Using Huygens' equivalence principle (or more specifically, the Stratton-Chu formulae [10]), one can find the following integral representations for the scattered electric and magnetic fields outside D,

$$-\frac{1}{i\omega\epsilon}\mathcal{D}(\boldsymbol{J})(\boldsymbol{r}) - \mathcal{K}(\boldsymbol{M})(\boldsymbol{r}) = \boldsymbol{E}^s(\boldsymbol{r}), \quad \boldsymbol{r} \in \mathrm{ext}(D), \tag{44}$$

$$-\frac{1}{i\omega\mu}\mathcal{D}(\boldsymbol{M})(\boldsymbol{r}) + \mathcal{K}(\boldsymbol{J})(\boldsymbol{r}) = \boldsymbol{H}^s(\boldsymbol{r}), \quad \boldsymbol{r} \in \mathrm{ext}(D), \tag{45}$$

where the equivalent surface currents $\boldsymbol{J}(\boldsymbol{r})$ and $\boldsymbol{M}(\boldsymbol{r})$ are tangential vector fields on the surface defined as, for $\boldsymbol{r} \in S$,

$$\boldsymbol{J}(\boldsymbol{r}) = \hat{\boldsymbol{n}}(\boldsymbol{r}) \times \boldsymbol{H}(\boldsymbol{r}), \tag{46}$$

$$\boldsymbol{M}(\boldsymbol{r}) = -\hat{\boldsymbol{n}}(\boldsymbol{r}) \times \boldsymbol{E}(\boldsymbol{r}). \tag{47}$$

where $\hat{\boldsymbol{n}}(\boldsymbol{r})$ is the outward directed unit normal of S. The total electric and magnetic fields are the sums of the known incident and the unknown scattered fields, i.e. $\boldsymbol{E}(\boldsymbol{r}) = \boldsymbol{E}^s(\boldsymbol{r}) + \boldsymbol{E}^i(\boldsymbol{r})$, $\boldsymbol{H}(\boldsymbol{r}) = \boldsymbol{H}^s(\boldsymbol{r}) + \boldsymbol{H}^i(\boldsymbol{r})$. In this surface integral formulation, the fields $\boldsymbol{E}^i(\boldsymbol{r})$ and $\boldsymbol{H}^i(\boldsymbol{r})$ are considered as the sources and the equivalent currents as the unknowns.

Furthermore, in (44) and (45) the integral operators $\mathcal{D}$ and $\mathcal{K}$ are defined for a continuous tangential vector field $\boldsymbol{F}(\boldsymbol{r})$ on the closed surface S with the help of the vector single layer potential $\mathcal{S}$, given by

$$\mathcal{S}(\boldsymbol{F})(\boldsymbol{r}) = \int_S G(\boldsymbol{r}, \boldsymbol{r}')\boldsymbol{F}(\boldsymbol{r}')\, dS', \tag{48}$$

where $G(\boldsymbol{r}, \boldsymbol{r}')$ is the scalar Green's function

$$G(\boldsymbol{r}, \boldsymbol{r}') = \frac{e^{ik|\boldsymbol{r}-\boldsymbol{r}'|}}{4\pi|\boldsymbol{r}-\boldsymbol{r}'|}. \tag{49}$$

Using $\mathcal{S}$, the double layer potential $\mathcal{K}$ can be written as

$$\mathcal{K}(\boldsymbol{F})(\boldsymbol{r}) = \nabla \times \mathcal{S}(\boldsymbol{F})(\boldsymbol{r}), \tag{50}$$

and $\mathcal{D}$ as

$$\mathcal{D}(\boldsymbol{F})(\boldsymbol{r}) = \nabla \times \mathcal{K}(\boldsymbol{F})(\boldsymbol{r}) = \nabla \times \nabla \times \mathcal{S}(\boldsymbol{F})(\boldsymbol{r}), \tag{51}$$

both for $\boldsymbol{r} \in \mathrm{ext}(D)$.

The presentations for the electric and the magnetic fields on the surface S are obtained by assuming that the point $\boldsymbol{r} \in \mathrm{ext}(D)$ in (44) and (45) is of the form $\boldsymbol{r} + h\hat{\boldsymbol{n}}(\boldsymbol{r})$, with $h > 0$, and then moving $\boldsymbol{r}$ to the surface S

by taking the limit as $h \to 0$. By taking the cross product of (51) with $\hat{\boldsymbol{n}}(\boldsymbol{r})$ and by moving the field point $\boldsymbol{r}$ to the surface S yields the following result [9],

$$\lim_{h\to 0} \hat{\boldsymbol{n}}(\boldsymbol{r}) \times \mathcal{D}(\boldsymbol{F})(\boldsymbol{r} + h\hat{\boldsymbol{n}}(\boldsymbol{r})) = \tilde{\mathcal{D}}(\boldsymbol{F})(\boldsymbol{r}) \\ = p.v. \int_S \hat{\boldsymbol{n}}(\boldsymbol{r}) \times (\nabla\times)^2 \left(G(\boldsymbol{r},\boldsymbol{r}')\boldsymbol{F}(\boldsymbol{r}')\right)\, dS', \quad (52)$$

where $p.v.$ stands for the principal value integral. Similarly, for the $\mathcal{K}$ operator we get

$$\lim_{h\to 0} \hat{\boldsymbol{n}}(\boldsymbol{r}) \times \mathcal{K}(\boldsymbol{F})(\boldsymbol{r} + h\hat{\boldsymbol{n}}(\boldsymbol{r})) = \tilde{\mathcal{K}}(\boldsymbol{F})(\boldsymbol{r}) + \frac{1}{2}\boldsymbol{F}(\boldsymbol{r}) \\ = \int_S \hat{\boldsymbol{n}}(\boldsymbol{r}) \times \nabla \times \left(G(\boldsymbol{r},\boldsymbol{r}')\boldsymbol{F}(\boldsymbol{r}')\right)\, dS' + \frac{1}{2}\boldsymbol{F}(\boldsymbol{r}). \quad (53)$$

By taking the cross products with $\hat{\boldsymbol{n}}(\boldsymbol{r})$ of both sides of (44) and of (45), inserting the limits (52) and (53), and replacing the scattered electric and magnetic fields by the difference of the total and incident fields, one obtains the familiar electric field integral equation (EFIE)

$$-\hat{\boldsymbol{n}}(\boldsymbol{r}) \times \boldsymbol{E}^i(\boldsymbol{r}) = -\frac{1}{i\omega\epsilon}\tilde{\mathcal{D}}(\boldsymbol{J})(\boldsymbol{r}) - \tilde{\mathcal{K}}(\boldsymbol{M})(\boldsymbol{r}) + \frac{1}{2}\boldsymbol{M}(\boldsymbol{r}), \quad \boldsymbol{r} \in S, \quad (54)$$

and the magnetic field integral equation (MFIE),

$$-\hat{\boldsymbol{n}}(\boldsymbol{r}) \times \boldsymbol{H}^i(\boldsymbol{r}) = -\frac{1}{i\omega\mu}\tilde{\mathcal{D}}(\boldsymbol{M})(\boldsymbol{r}) + \tilde{\mathcal{K}}(\boldsymbol{J})(\boldsymbol{r}) - \frac{1}{2}\boldsymbol{J}(\boldsymbol{r}), \quad \boldsymbol{r} \in S. \quad (55)$$

In the equations (54) and (55) the unknowns are the electric and magnetic surface currents $\boldsymbol{J}$ and $\boldsymbol{M}$. If an IBC of type (13) is valid on S, we can eliminate either $\boldsymbol{J}$ or $\boldsymbol{M}$ from one of the equations (54)-(55), and we only need to solve one equation for one unknown. For example, for a PEC surface the boundary condition indicates that the tangential components of the total electric field are zero on the surface, i.e.

$$\hat{\boldsymbol{n}}(\boldsymbol{r}) \times \boldsymbol{E}(\boldsymbol{r}) = -\boldsymbol{M}(\boldsymbol{r}) = 0, \quad (56)$$

in which case the all the terms containing the magnetic surface current $\boldsymbol{M}$ can be eliminated.

3.2 Method of Moments

Method of Moments (MoM), sometimes also called the generalized Galerkin method, is often used for numerically solving equations of following type,

$$\mathcal{L}\boldsymbol{J} = \boldsymbol{E}, \quad (57)$$

where $\boldsymbol{E}$ is the known electric field, $\boldsymbol{J}$ is the unknown current density and $\mathcal{L}$ is a linear (integral) operator, for example one of the operators $\mathcal{S}$, $\mathcal{D}$, or $\mathcal{K}$. The first step in the method is to expand the unknown current density $\boldsymbol{J}$ by the basis functions $\boldsymbol{j}_n$

$$\boldsymbol{J} \approx \sum_{n=1}^{N} x_n \boldsymbol{j}_n, \tag{58}$$

where $x_n \in \mathbb{C}$ are unknown coefficients. Inserting this into (57) gives us

$$\sum_{n=1}^{N} x_n \mathcal{L}\boldsymbol{j}_n \approx \boldsymbol{E}, \tag{59}$$

or, by subtracting the approximation (59) from (57), one gets

$$\mathcal{L}\boldsymbol{J} - \sum_{n=1}^{N} x_n \mathcal{L}\boldsymbol{j}_n = \boldsymbol{E} - \sum_{n=1}^{N} x_n \mathcal{L}\boldsymbol{j}_n, \tag{60}$$

where the left-hand side is called the residual $\boldsymbol{R}$.

The residual $\boldsymbol{R}$ is then minimized in the space spanned by the testing functions $\boldsymbol{t}_m$, $m = 1, \ldots, N$, so that it is orthogonal to all testing functions $\boldsymbol{t}_m$. Orthogonality is measured by a product $\langle \cdot\,, \cdot \rangle$, which gives us

$$\langle \boldsymbol{t}_m, \boldsymbol{R} \rangle = 0 = \langle \boldsymbol{t}_m, \boldsymbol{E} \rangle - \sum_{n=1}^{N} x_n \langle \boldsymbol{t}_m, \mathcal{L}\boldsymbol{j}_n \rangle, \quad m = 1, \ldots, N. \tag{61}$$

where the product $\langle \cdot, \cdot \rangle$ is defined as

$$\langle \boldsymbol{g}, \boldsymbol{f} \rangle = \int_S \boldsymbol{g}(\boldsymbol{r}) \cdot \boldsymbol{f}(\boldsymbol{r})\, dS. \tag{62}$$

Often the set of basis functions is chosen as the set of testing functions, in which case the MoM formulation is equivalent to the usual Galerkin method.

Triangular rooftop functions, also known as Rao-Wilton-Glisson (RWG) functions [54], are a popular choice for basis and testing functions. For triangular surface elements T^+ and T^-, which share a common edge I_n (or I_m), these functions can be written as

$$\boldsymbol{f}_n(\boldsymbol{r}) = \begin{cases} \dfrac{L}{2A^+}(\boldsymbol{r} - \boldsymbol{p}^+), & \text{if } \boldsymbol{r} \in T^+, \\ -\dfrac{L}{2A^-}(\boldsymbol{r} - \boldsymbol{p}^-), & \text{if } \boldsymbol{r} \in T^-, \\ 0, & \text{otherwise,} \end{cases} \tag{63}$$

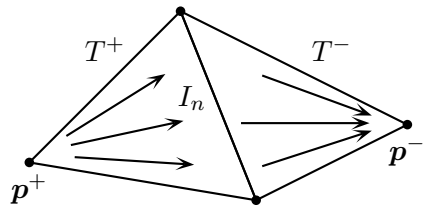

Figure 9: RWG functions are defined for a pair of adjacent triangles.

where L is the length of the edge I_n, A^+ and A^- are the areas of T^+ and T^-, respectively, and $\boldsymbol{p}^+$ and $\boldsymbol{p}^-$ are the vertices of T^+ and T^- which are opposite to I_n. According to the definition, the current density flows from element T^+ to element T^- (see Fig. 9).

The rooftop functions are also very commonly used as basis functions in MoM formulations. They are particularly well suited for modeling large planar structures that have straight edges. The rooftop functions are defined for a pair of adjacent rectangles P^+ and P^-, which share a common edge I_n, with the help of the shape function $s_n(\boldsymbol{r})$ defined by

$$s_n(\boldsymbol{r}) = \begin{cases} \dfrac{L}{A^+}(\boldsymbol{r} - \boldsymbol{p}^+) \cdot \hat{\boldsymbol{u}}^+, & \text{if } \boldsymbol{r} \in P^+, \\ -\dfrac{L}{A^-}(\boldsymbol{r} - \boldsymbol{p}^-) \cdot \hat{\boldsymbol{u}}^-, & \text{if } \boldsymbol{r} \in P^-, \\ 0, & \text{otherwise}, \end{cases} \tag{64}$$

where L is the length of the edge I_n, A^+ and A^- are the areas of P^+ and P^-, respectively, and $\boldsymbol{p}^+$, $\boldsymbol{p}^-$ and the unit vectors $\hat{\boldsymbol{u}}^+$, $\hat{\boldsymbol{u}}^-$ are as in Fig. 10. The constants L/A^+ and L/A^- can also be written as $L/A^+ = 1/L^+$ and $L/A^- = 1/L^-$. The basis functions are then defined using the shape functions,

$$\boldsymbol{f}_n(\boldsymbol{r}) = s_n(\boldsymbol{r})\hat{\boldsymbol{u}}, \tag{65}$$

where $\hat{\boldsymbol{u}} = \hat{\boldsymbol{u}}^+$ for $\boldsymbol{r} \in P^+$ and $\hat{\boldsymbol{u}} = \hat{\boldsymbol{u}}^-$ for $\boldsymbol{r} \in P^-$.

RWG and rooftop functions have the property that their normal component is continuous across the edge I_n, i.e. they are divergence conforming. Also, it is worth noting that on the other edges of the elements T^+ and T^- (or P^+ and P^-), the current is always tangential to the boundary and is zero on the vertices. Thus, the net current flowing out from or in to the elements is zero.

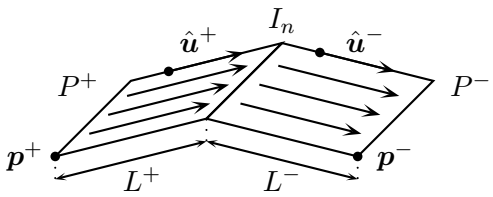

Figure 10: Rooftop functions are defined for a pair of adjacent rectangles.

3.3 Accurate Numerical Integration

In the Method of Moments formulation, the discretized surface integral equations are used to compute the system matrix elements A_{mn} from double integrals of the following type,

$$A_{mn} = \int_{S_m} \boldsymbol{t}_m(\boldsymbol{r}) \cdot \left(\mathcal{L}(\boldsymbol{b}_n)(\boldsymbol{r}') \right) \, dS, \tag{66}$$

where the linear operator $\mathcal{L}(f)$ may be any of the above defined integral operators $\mathcal{S}(f)$, $\mathcal{K}(f)$, or $\mathcal{D}(f)$. The outer and inner integrals above are evaluated on the surface patches S_m and S_n where the testing and the basis functions are defined.

When these surface patches overlap or touch each other, the inner integral in (66) may be singular. Accurate evaluation of these singular integrals is quite difficult, and several different methods have been proposed to efficiently compute them. These accurate methods may also be used in the near-singular cases, where the surface patches are close to each other, i.e. the distance between the evaluation point $\boldsymbol{r}$ and the source point $\boldsymbol{r}'$ is small, since otherwise the number of integration points in the numerical integration rules required for accurate integration may become too large.

These accurate integration methods include, for example, the so-called singularity cancellation methods that are based on coordinate transformation techniques, e.g. the polar transformation technique, the Duffy's transformation [12, 71], and the recent Khayat-Wilton method [32, 70]. In the articles of this thesis the evaluation of these singular and near-singular integrals has been based on the singularity subtraction technique with closed-form integral representations [4, 13, 22, 72, 80, 83].

The singularity subtraction technique is based on the Taylor series of the exponential function in the Green's function. The exponential is expanded at $R = |\boldsymbol{r} - \boldsymbol{r}'| = 0$,

$$e^{ikR} = \sum_{q=0}^{\infty} \frac{(ikR)^q}{q!} = 1 + ikR - \frac{k^2R^2}{2} - \frac{ik^3R^3}{6} + \ldots \tag{67}$$

so that the free space Green's function, with the above expansion, can then be written

$$G(\boldsymbol{r},\boldsymbol{r}') = \frac{1}{4\pi}\sum_{q=-1}^{\infty}\frac{(ik)^{q+1}R^q}{(q+1)!} = \frac{1}{4\pi}\left(\frac{1}{R} + ik - \frac{k^2R}{2} - \frac{ik^2R^2}{6} + \ldots\right) \tag{68}$$

In the expansion (68) the problematic terms regarding the numerical integration are the "odd" terms ($q = -1, 1, 3, \ldots$), which are not smooth. The first term is of course singular, and is subtracted from the series. However, even with the first term removed, the derivative of the remaining series is discontinuous at $R = 0$, so the numerical integration may still not be accurate in all cases. Therefore more "odd" terms than one need to be removed for an accurate evaluation of the integrals [83].

In practical implementations, the singular integrals are then split into smooth and non-smooth parts, e.g.

$$\begin{aligned}&\int_{S_n} G(\boldsymbol{r},\boldsymbol{r}')\boldsymbol{b}_n(\boldsymbol{r}')\,dS' \\ &= \int_{S_n} G_s(\boldsymbol{r},\boldsymbol{r}')\boldsymbol{b}_n(\boldsymbol{r}')\,dS' + \frac{1}{4\pi}\int_{S_n}\frac{1}{R}\boldsymbol{b}_n(\boldsymbol{r}')\,dS' - \frac{k^2}{8\pi}\int_{S_n} R\boldsymbol{b}_n(\boldsymbol{r}')\,dS',\end{aligned} \tag{69}$$

where the "smooth" Green's function $G_s(\boldsymbol{r},\boldsymbol{r}')$ is the original Green's function with the first two "odd" terms removed,

$$G_s(\boldsymbol{r},\boldsymbol{r}') = \frac{1}{4\pi}\left(\frac{e^{ikR}-1}{R} + \frac{k^2R}{2}\right). \tag{70}$$

More "odd" terms may be removed if accurate integration so requires. However, since the product kR is small, the higher powers of kR diminish very quickly, so in practical computations subtracting only the first two odd terms ($q = -1$ and $q = 1$) turns out to be sufficient.

The smooth part of the integral may then be evaluated numerically, e.g. using Gaussian quadratures. The non-smooth integrals of the odd powers of R^q can be reduced, through vector algebra and by using basic integral identities, to the line and surface integrals of the following types

$$I_L^q(\Delta L) = \int_{\Delta L} R^q\,dl', \tag{71}$$

and

$$I_S^q(S) = \int_S R^q\,dS', \tag{72}$$

where ΔL is one edge of the integration element, and S is the surface area. The integrals (71) and (72) can be further reduced to lower order line and

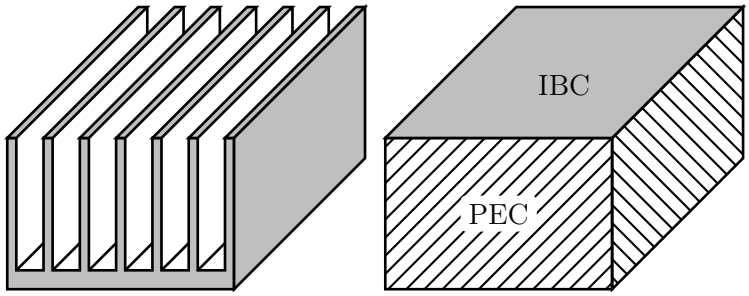

Figure 11: Corrugated surface may be replaced by an IBC if the dimensions of the corrugation are suitable.

surface integrals using recursive integration rules. Recursion is used until the order R^{-3} for surface integrals and R^{-1} for line integrals is reached. For these powers, the integrals may be evaluated analytically, as shown in [P3].

The recursive integration rules are derived in detail for RWG and rooftop functions in [P3]. As these integration rules are usually somewhat different for each basis function type, they must be derived separately for each case. However, if the basis functions can be expressed in a more general form, for example by using polynomial shape functions, then these rules can be derived in a more general way [28, 29].

4 Scattering from Anisotropic Surfaces

In papers [P4] and [P5] the scattering properties of two kinds of anisotropic surfaces are studied using MoM and IBC. Both these surfaces can be realized by a corrugated surface (see Fig. 11). Previously, numerical methods and formulations for anisotropic impedance surfaces have been introduced, see e.g. [21, 38], but these are applicable only for cases where the impedance values are small.

For a corrugated surface whose properties closely resemble those of an SHS, as is the case in [P4] and [P5], the IBC assumes either very small or very high impedance values, depending on the direction of the fields on the surface. This means that some physical interpretation that takes into account the behavior of the equivalent currents on the studied surfaces must be used when formulating the problem.

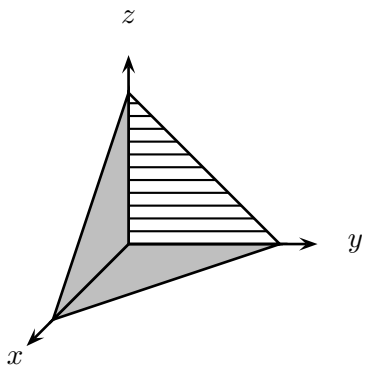

Figure 12: Trihedral corner reflector with an interior corrugated face.

4.1 Scattering from Soft-and-Hard Surface

Trihedral corner reflectors are often used in remote sensing and radar technology as location markers and calibration targets [49, 62], since they have a high backscattering radar cross section over a wide angular range, are easy to construct, and do not require any power to operate.

In [P4] a trihedral corner reflector that has one or several corrugated interior faces was studied (see Fig. 12). The corrugation was assumed to be perfectly tuned to the incident wave frequency, in which case the impedance values in (31) and (32) become $Z_u \to 0$ and $Z_v \to \infty$. Then the corrugation can be considered to approximate an SHS, so that the boundary condition on these interior faces is the SHS boundary condition (23).

The use of an SHS on one or several of the interior faces of the trihedral corner reflector opens up the interesting possibility to construct such a reflector that the reflected wave has the same handedness as the incident elliptically polarized field, or that the reflected field is rotated by 90° in the case of linearly polarized incident field. This property makes the reflected field easier to distinguish from the background noise due to the environment.

The scattering properties of an SHS corner reflector have been previously studied, but the methods used in these studies were not as accurate as a full MoM computation [20, 45]. Other methods for analyzing corrugated and Soft-and-Hard surfaces have also been introduced [36, 37, 39, 64, 82], but these are somewhat complex and computationally intensive compared to the method presented in [P4].

As can be seen from the SHS boundary condition (23), on such a

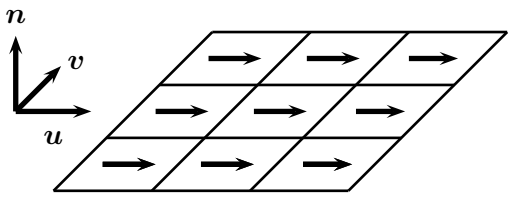

Figure 13: Configuring the rooftop functions so that they only allow current flow to the $\hat{\boldsymbol{u}}$-direction, i.e. the direction of the corrugation, directly fulfills the SHS boundary condition.

surface the equivalent electric and magnetic surface currents can only flow in the $\hat{\boldsymbol{u}}$-direction, i.e.

$$\boldsymbol{J} = \hat{\boldsymbol{n}} \times \boldsymbol{H} = \hat{\boldsymbol{n}} \times (H_u \hat{\boldsymbol{u}} + H_v \hat{\boldsymbol{v}} + H_n \hat{\boldsymbol{n}}) = -H_v \hat{\boldsymbol{u}}, \tag{73}$$

and

$$\boldsymbol{M} = -\hat{\boldsymbol{n}} \times \boldsymbol{E} = -\hat{\boldsymbol{n}} \times (E_u \hat{\boldsymbol{u}} + E_v \hat{\boldsymbol{v}} + E_n \hat{\boldsymbol{n}}) = E_v \hat{\boldsymbol{u}}, \tag{74}$$

with $\hat{\boldsymbol{u}} \times \hat{\boldsymbol{v}} = \hat{\boldsymbol{n}}$. Accordingly, the configuration of basis functions must be such that they model this unidirectional current behavior in a physically correct way. The popularly used RWG functions (63) are in this case a bad choice, as forcing this kind of a current behavior leads to the use of infinite and zero impedance values according to (31) and (32).

However, rooftop functions (65) can easily be made to mimic the correct currents, so they were used instead. This also led to the necessary task of deriving the singularity subtraction formulae for the rooftop functions that were discussed in the Section 3.

As the SHS boundary imposes a condition for both the electric and the magnetic field, both the electric and magnetic field integral equations must be used. Using the boundary conditions (73) and (74) in the EFIE (54) and MFIE (55) then yields the integral equations that are needed to solve the unknown electric and magnetic surface currents on the SHS.

Using the rooftop functions also allows one to easily take into account the SHS boundary condition in the integral equation formulation. Configuring the basis functions on the SHS so that they only allow current flow to the $\hat{\boldsymbol{u}}$-direction means that the the boundary condition is automatically fulfilled on the surface (see Fig. 13). This also lowers the computational cost of modeling an SHS, since the number of needed basis functions is essentially half of that of the corresponding PEC surface. These insights are the major novelties in the paper [P4].

4.2 Scattering from Anisotropic Impedance Boundary

As the SHS is only applicable as an approximate boundary for perfectly tuned corrugated surfaces, it was of interest to study how it would be possible to extend the implementation presented in [P4] to corrugations that deviate slightly from the perfectly tuned one. In [P5] an IBC was derived that can be applied to such corrugated surfaces.

The problem, as explained above, is that it is not possible to use the usual IBC (13), as the impedance and admittance values for the corrugation (31) and (32) will have at least one very large value. Also, at the limit where the geometry of the corrugation approaches the SHS case, the IBC should return the SHS boundary condition.

Thus, instead of using only the impedance or admittance in the IBC, only those components which have a very small value in the chosen configuration are used. The IBC for approximating corrugations that closely resemble the perfectly tuned one can then be written in the form

$$\hat{\boldsymbol{u}} \cdot \boldsymbol{E} = -Z_u \hat{\boldsymbol{v}} \cdot \boldsymbol{H}, \quad \hat{\boldsymbol{u}} \cdot \boldsymbol{H} = Y_v \hat{\boldsymbol{v}} \cdot \boldsymbol{E}, \tag{75}$$

which is more suited to numerical computations, and also returns the SHS boundary condition as the limit $Z_u \to 0$, $Z_v \to \infty$. As in [P4], the equivalent surface currents are best modeled using rooftop functions as basis functions in the MoM solution.

The impedance and admittance values for the corrugation in (75) can be computed using (31) and (32). Although these values are strictly speaking only valid for normal incidence, numerical analysis using an exact two dimensional corrugation model has shown that they are nevertheless a good approximation for the real values even for oblique incidence [74].

According to (75), in addition to the $\hat{\boldsymbol{u}}$-directional equivalent surface currents, there are now also small perturbation type currents that are perpendicular to the dominant direction, i.e.

$$\boldsymbol{J} = -\hat{\boldsymbol{n}} \times (Y_v E_v \hat{\boldsymbol{u}} + H_v \hat{\boldsymbol{v}} + H_n \hat{\boldsymbol{n}}) = H_v \hat{\boldsymbol{u}} - Y_v E_v \hat{\boldsymbol{v}} \tag{76}$$

and

$$\boldsymbol{M} = \hat{\boldsymbol{n}} \times (-Z_u H_v \hat{\boldsymbol{u}} + E_v \hat{\boldsymbol{v}} + E_n \hat{\boldsymbol{n}}) = -E_v \hat{\boldsymbol{u}} + Z_u H_v \hat{\boldsymbol{v}} \tag{77}$$

The basis functions must now allow current flow to both the $\hat{\boldsymbol{u}}$- and the $\hat{\boldsymbol{v}}$-direction. The $\hat{\boldsymbol{v}}$-directional currents are multiplied by the proper impedance or the admittance values, so that the current behavior is as shown in the Fig. 14. Again, inserting the equations (76) and (77) into the EFIE (54) and the MFIE (55), yields the needed integral equation formulations.

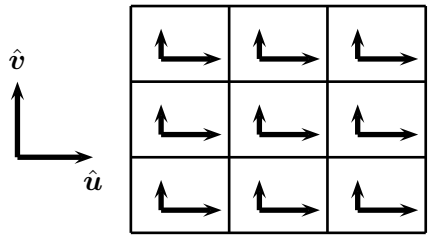

Figure 14: On the impedance boundary that closely resembles a corrugated surface, in addition to the dominant $\hat{\boldsymbol{u}}$-directional currents, there are also small $\hat{\boldsymbol{v}}$-directional currents that need to be taken into account.

The scale of these small $\hat{\boldsymbol{v}}$-directional currents is dictated by the impedance and admittance values, which can not be made very large. The impedance and admittance values are, in turn, dictated by the geometrical properties of the corrugation.

If the impedance or admittance values become too large in comparison to the ideal SHS case, the numerical accuracy of the method is lost, as the numerical computations in [P5] show. Also, the accuracy of the method suffers when modeling scattering from corrugated surfaces in scattering and incident directions that are too close to the tangent plane.

5 Multilevel Fast Multipole Algorithm

An IBC can be used in scattering computations to replace a complicated surface by a simpler one, as discussed in the previous sections. Verifying that these simplifications correctly model the original scatterer often means that the full scattering problem must be solved, which may be computationally a very expensive operation. For this reason, fast and efficient numerical methods are an interesting research subject that is closely related to the analysis of anisotropic impedance surfaces.

Solving scattering problems based on integral equations involves either inverting a full system matrix or alternatively using an iterative solution method. For direct solvers, such as Gaussian elimination or lower-upper-triangular decomposition, the computational complexity is proportional to $\mathcal{O}(N^3)$, where N is the number of unknowns.

The computational cost of iterative solvers is of the order $\mathcal{O}(N^2)$, which can still be very large. The Fast Multipole Method (FMM) was developed to speed up the iterative solution methods. The original FMM

for static problems was introduced by Greengard and Rokhlin [23]. A version suitable for solving high frequency problems using the Helmholtz equation was later developed by Rokhlin et al. [7, 14, 15, 55, 56], which reduced the computational cost to $\mathcal{O}(N^{1.5})$.

Shortly thereafter a multilevel version (Multilevel Fast Multipole Algorithm, MLFMA) was presented [5, 6, 66, 67], which further reduces the computational cost of using iterative solvers to $\mathcal{O}(N \log N)$. The MLFMA has been extensively studied during the last decade, and it is considered to be one of the most important computational algorithms available for electromagnetic scattering computations [2, 11]. It has been used to solve scattering problems involving a significant number of unknowns [24, 75], and the development of the algorithm is still ongoing, see e.g. [16, 18, 77, 78]

5.1 Background

To illustrate the concepts of the FMM and the MLFMA, consider the basic scattering problem shown in the Fig. 8. When using MoM to solve the scattering problem, the surface S is first discretized into N sufficiently small surface elements, for example triangular or rectangular patches. Then the system matrix elements A_{mn} are computed from an equation of the form (66). The result is a matrix-vector equation

$$\sum_{n=1}^{N} A_{mn} x_n = F_m, \quad m = 1, \ldots, N, \tag{78}$$

where x_n are the unknown coefficients of the basis functions, and the right hand side vector is computed by

$$F_m = \int_S \boldsymbol{t}_m \cdot \boldsymbol{F}^i \, dS, \tag{79}$$

where $\boldsymbol{F}^i$ is the incident field.

Using matrix inversion or other direct methods to solve the equation (78) incurs a cost of order $\mathcal{O}(N^3)$. Due to the high cost of direct solvers, iterative solution methods, such as the GMRES or the conjugate gradient method, which have a computational cost of order $\mathcal{O}(N^2)$, are often used instead. The FMM and the MLFMA can be used to speed up the computing of the matrix-vector products in the iterative solution methods lowering the cost to order $\mathcal{O}(N^{1.5})$ and $\mathcal{O}(N \log N)$, respectively.

In the FMM and the MLFMA, the full system matrix is never computed. Instead, the interactions between elements are computed using a three-step procedure that is explained below. First, the discretized surface

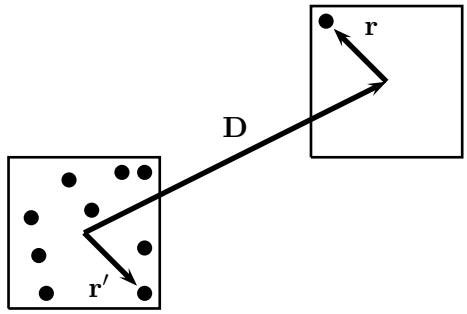

Figure 15: The out-to-in translation converts the outgoing field from the source cube to the incoming field in the target cube.

elements are grouped inside the cubes. After that, the cubes are divided into nearby and well separated cubes, so that for each cube its nearby cubes are those that share with it at least one boundary point.

The matrix-vector products are then redistributed between the nearby and the well-separated cubes, so that

$$\sum_{n=1}^{N} A_{mn}x_n = \sum_{n\in G} A_{mn}x_n + \sum_{n\notin G} A_{mn}x_n, \quad m = 1,\ldots,N, \tag{80}$$

where G is the group of all elements that belong to the nearby cubes. Only the interactions between elements that belong to the nearby cubes are computed using the regular MoM matrix elements. The matrix-vector products for the well separated cubes are computed in a fast way. To simplify the analysis, let us only consider the case shown in Fig. 15 that only involves one source cube centered at the origin, one target cube centered at $\boldsymbol{D}$, and the matrix elements of the following type,

$$A_{mn} = \int_S \boldsymbol{t}_m(\boldsymbol{r}) \cdot \left(\int_{S'} G(\boldsymbol{r},\boldsymbol{r}')\boldsymbol{b}_n(\boldsymbol{r}')\, dS' \right) dS. \tag{81}$$

The FMM and the MLFMA are based on the plane-wave expansion of the Green's function (49), which is obtained from the truncated multipole series expansion of the Green's function [6]. Inserting the plane-wave expansion into the equation (81), and changing the order of integration gives for the inner integral the approximation

$$\int_{S'} G(\boldsymbol{r},\boldsymbol{r}')\boldsymbol{b}_n(\boldsymbol{r}')\, dS' \simeq \int_{|\hat{\boldsymbol{k}}|=1} e^{ik\hat{\boldsymbol{k}}\cdot\boldsymbol{r}} T_L(\boldsymbol{D},\hat{\boldsymbol{k}}) F_{n,\infty}(\hat{\boldsymbol{k}})\, d\hat{\boldsymbol{k}} \tag{82}$$

where $F_{n,\infty}(\hat{\boldsymbol{k}})$ is the far field pattern due to the basis function $\boldsymbol{b}_n$,

$$F_{n,\infty}(\hat{\boldsymbol{k}}) = \frac{1}{4\pi} \int_S e^{-ik\hat{\boldsymbol{k}}\cdot\boldsymbol{r}'} \boldsymbol{b}_n(\boldsymbol{r}')\, dS', \tag{83}$$

T_L is the Rokhlin translator of order L,

$$T_L(\boldsymbol{D}, \hat{\boldsymbol{k}}) = \frac{ik}{4\pi} \sum_{n=0}^{L} i^n (2n+1) h_n^{(1)}(kD) P_n(\hat{\boldsymbol{k}} \cdot \hat{\boldsymbol{D}}), \tag{84}$$

$h_n^{(1)}(x)$ is the spherical Hankel function of the first kind, $P_n(x)$ is the Legendre polynomial, and $|\boldsymbol{r} - \boldsymbol{r}'| < |\boldsymbol{D}|$. The vector $\boldsymbol{D}$ is called the translation vector. The order L in (84) controls the approximation error (also called the truncation error) in the equation (82).

Using the procedure explained above, one can compute the matrix-vector products in (80) as follows. First compute the far field patterns due to the basis functions in division cubes on each division level, see below. Then, using the Rokhlin translator (84) compute the so-called out-to-in translations from the source cubes to the field cubes, which convert the outgoing fields, given by the radiation pattern $F_{n,\infty}(\hat{\boldsymbol{k}})$, to incoming fields, given by the incoming wave pattern $V(\hat{\boldsymbol{k}})$, inside the field cubes,

$$V(\hat{\boldsymbol{k}}) = T_L(\boldsymbol{D}, \hat{\boldsymbol{k}}) \left(\sum_n x_n F_{n,\infty}(\hat{\boldsymbol{k}}) \right). \tag{85}$$

The matrix-vector products for the well-separated cubes on the lowest division level can then be computed by

$$\sum_{n \notin G} A_{mn} x_n \simeq \int_S \boldsymbol{t}_m(\boldsymbol{r}) \cdot \left(\int_{|\hat{\boldsymbol{k}}|=1} V(\hat{\boldsymbol{k}}) e^{ik\hat{\boldsymbol{k}}\cdot\boldsymbol{r}}\, d\hat{\boldsymbol{k}} \right) dS. \tag{86}$$

5.2 Overview of the MLFMA

When solving a surface integral equation with MLFMA and MoM, the scatterer is first divided into cubes that have a sidelength $a_l = 2^{l-1}\lambda$. After that the cubes on the lowest division level l are grouped inside cubes on the next level $l+1$, so that on this level the cubes contain eight lower level cubes each. The lower level (child) cubes are grouped inside larger (parent) cubes on the higher level until the highest level, where at least two non-empty well separated cubes still appear, is reached.

The discretized surface elements are grouped inside the cubes on the lowest level so that each cube contains a small number of elements, say between ten and one hundred, or is empty. Only non-empty cubes are listed.

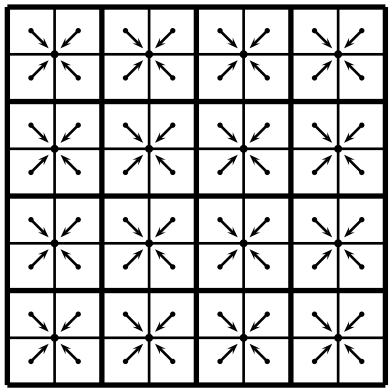

Figure 16: In the aggregation stage, all the contributions from the child cubes are grouped together in the parent cube.

Two cubes that are on the same level and share at least one boundary point are called nearby cubes. Two cubes that are not nearby and are on the same level are well separated. The interaction list of a cube contains other cubes on the same level that are well separated and are contained in the nearby cubes of the parent cube.

The MLFMA can be separated into three separate parts: preprocessing, aggregation, and disaggregation. In the preprocessing part, which includes the discretization and division process described above, the far field patterns of each surface element are computed using (83).

In the aggregation phase, the far field patterns for each cube on each division level are computed, starting from the lowest level. On the lowest level, the previously computed element far field patters are summed together to form the far field field pattern $W_l(\hat{\boldsymbol{k}})$ of each cube (see Fig. 16). Continuing up to the next level $l+1$, these are then transformed and summed into far field patterns $W_{l+1}(\hat{\boldsymbol{k}})$ of the higher level parent cubes using the out-to-out translation,

$$W_{l+1}(\hat{\boldsymbol{k}}) = e^{ik\hat{\boldsymbol{k}}\cdot(\boldsymbol{r}_l - \boldsymbol{r}_{l+1})} W_l(\hat{\boldsymbol{k}}), \tag{87}$$

where $\boldsymbol{r}_l$ is the center of the division cube on the level l. The algorithm continues in this fashion until the highest division level is reached.

In the disaggregation phase, the far field patterns are translated into incoming field patterns and then disaggregated. On the highest division level, the incoming fields $V_l(\hat{\boldsymbol{k}})$ for each cube are computed from the far

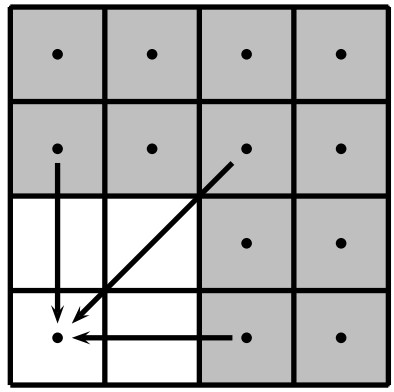

Figure 17: On the highest level the contributions from the well separated (shaded) cubes are translated to the target cube.

field patterns $W_l(\hat{\boldsymbol{k}})$ of well separated cubes using the out-to-in translation (85) (see Fig. 17).

Continuing to the second to highest level, the incoming fields $V_{l-1}(\hat{\boldsymbol{k}})$ are computed from the cubes in the interaction list of each cube using the out-to-in translation and also from the incoming field patterns $V_l(\hat{\boldsymbol{k}})$ of the parent cube using the in-to-in translation (see Fig. 18),

$$V_{l-1}(\hat{\boldsymbol{k}}) = e^{ik\hat{\boldsymbol{k}}\cdot(\boldsymbol{r}_l - \boldsymbol{r}_{l-1})} V_l(\hat{\boldsymbol{k}}). \tag{88}$$

The algorithm continues in this fashion until the lowest division level is reached.

On the lowest level, the final values are then computed using (86). The interactions of the surface elements inside the same and the nearby division cubes must also be taken into account. These interactions are computed using the regular MoM formulation.

5.3 Efficient Evaluation of the Rokhlin Translator

In the numerical evaluation of the integral (86), the Rokhlin translator T_L must first be sampled in the directions $\hat{\boldsymbol{k}}_{mn}$ dictated by the used integration rule. As the number of these sampling directions depends on the order L of the Rokhlin translator, the associated computational costs, i.e. the processing time and the storage cost, may be significant especially on the higher division levels when L is large.

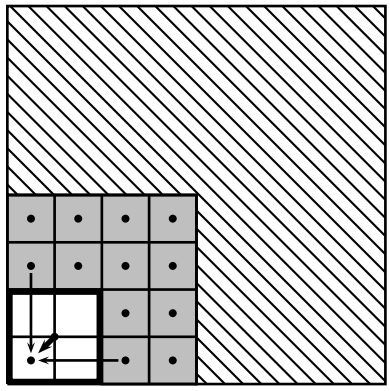

Figure 18: On level $l-1$ the contributions of the cubes in the interaction list (shaded cubes) are taken into account and the effect of the l level cubes well separated from the parent cube (hatched cubes) are computed from the incoming field pattern of the parent cube.

It is possible to considerably decrease these computational costs by using Lagrange interpolation to evaluate the Rokhlin transfer function, as has been demonstrated by several authors [17, 40, 65]. An accurate interpolation method requires that the oversampling factor s and the number of points in the interpolation stencil $2p$ are sufficiently high for the target accuracy (see Fig. 19).

As the number of the directions $\hat{\boldsymbol{k}}_{mn}$ where the values of T_L must be computed is high, also the number of needed interpolations is very large. To obtain the computationally most efficient interpolation method, the number of the stencil points in the interpolation must be minimized. This can be achieved by using a high oversampling factor (see Fig. 20).

However, the use of a high oversampling factor increases the computational and, especially, the storage costs required by the direct oversampling. It is thus essential to find such values for the oversampling factor and for the number of stencil points that are sufficient for the target accuracy and are the computationally most efficient.

In [P6] it is shown by using the Fast Fourier Transform (FFT) based oversampling method for the Rokhlin translator T_L, that it is possible to considerably decrease the computational costs associated with the interpolation method. The FFT technique allows the use of much larger oversampling factors without increasing the storage costs. Thus the num-

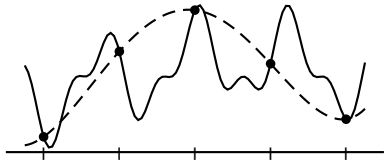

Figure 19: If the density of the sample points is not sufficient, the number of the stencil points must be increased in order to accurately integrate a highly oscillating function.

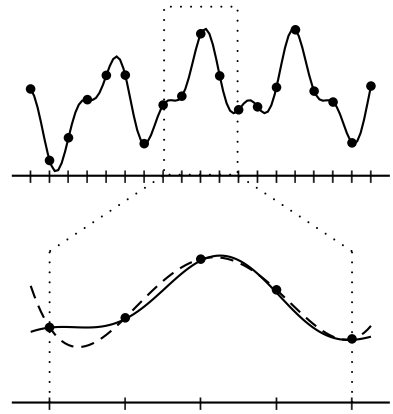

Figure 20: By oversampling the original function the number of the stencil points may be reduced, as a lower order polynomial is sufficient for accurate interpolation.

ber of stencil points can be reduced, which decreases the computational costs. These improvements significantly increase the efficiency of the interpolation algorithm. The FFT technique has also been used to speed up the computations in the aggregation and the disaggregation stages of the MLFMA [59].

The interpolation technique is based on the fact that $T_L(\boldsymbol{D}, \hat{\boldsymbol{k}})$ is a trigonometric polynomial $T_L(\alpha)$ of order L, with $\alpha = \arccos(\hat{\boldsymbol{D}} \cdot \hat{\boldsymbol{k}})$,

$$T_L(\alpha) = \sum_{n=-L}^{L} b_n e^{in\alpha}, \quad -\pi \leq \alpha \leq \pi. \tag{89}$$

This can be seen from the equation (84), since P_n is the Legendre polynomial of degree n and its argument can be written in the form $\hat{\boldsymbol{D}} \cdot \hat{\boldsymbol{k}} = \cos\alpha = \frac{1}{2}\left(e^{i\alpha} + e^{-i\alpha}\right)$.

Using the Lagrange interpolation, the values of T_L can be computed by

$$\tilde{T}_L(\alpha) = \sum_{j=1}^{2p} T_L(\beta_j)\gamma_j(\alpha), \tag{90}$$

where $\tilde{T}_L(\alpha)$ is the interpolate of T_L, and the interpolating polynomials

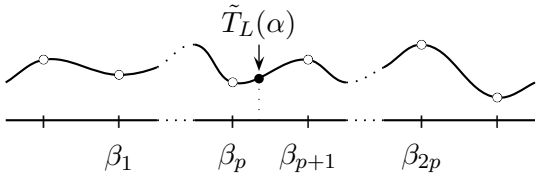

Figure 21: The stencil points are evenly distributed on both sides of the interpolation point in the Lagrange interpolation.

$\gamma_j(\alpha)$ are defined as

$$\gamma_j(\alpha) = \prod_{\substack{k=1 \\ k\neq j}}^{2p} \frac{\alpha - \beta_k}{\beta_j - \beta_k} \tag{91}$$

The interpolation stencil points are $\beta_j = \alpha_{m+j}$, $j = 1, \ldots, 2p$, with m chosen so that $\beta_p \leq \alpha \leq \beta_{p+1}$, i.e. the interpolation point α is in the center interval of the stencil (see Fig. 21).

To use the FFT based oversampling method for the interpolation, the samples are first computed directly in the Nyquist sampling points

$$\alpha'_m = \frac{2\pi}{2L+1} m, \quad m = -L, \ldots, L. \tag{92}$$

by (84)

$$u(m) = T_L(\alpha'_m). \tag{93}$$

Then the centered Fourier transform $\mathcal{F}_{2L+1}$,

$$\left(\mathcal{F}_{2L+1} u\right)(n) = \sum_{m=-L}^{L} u(m) e^{-i\frac{2\pi}{2L+1}nm}, \quad n = -L, \ldots, L, \tag{94}$$

is used to compute the coefficients $b_n = b(n)$ in (89) by

$$b(n) = \frac{1}{2L+1} \left(\mathcal{F}_{2L+1} u\right)(n), \quad n = -L, \ldots, L. \tag{95}$$

The oversampling is achieved simply by zero-padding the sequence b, i.e. by adding $sL - L$ zeros at both ends of b to get the sequence c, and then computing the values $T_L(\alpha_m)$ in the oversampling points α_m by the inverse Fourier transform $\mathcal{F}^{-1}_{2sL+1}$ as

$$T_L(\alpha_m) = (2sL+1) \left(\mathcal{F}^{-1}_{2sL+1} c\right)(m), \quad m = -sL, \ldots, sL. \tag{96}$$

The computational cost of using FFT in (95) and (96) is of the order $2sL\log(2sL)$, which is significantly faster than direct oversampling. Also, when using the FFT technique the oversampled values need not be computed and stored beforehand, so the memory costs can be minimized. As it is essential to find the optimal values for the interpolation parameters for a fast algorithm, i.e. the oversampling factor s and the number of stencil points $2p$, in [P6] these values are found using both a numerical search and an analytical upper bound for the field error.

The order L of the Rohklin translator T_L plays a significant role in the accuracy and the computational cost of the MLFMA, so it is important that the value for L is chosen correctly. The order L can be accurately obtained by computing the truncation error in the incoming multipole series of the Green's function, see e.g. [6]. In [P6], these orders are found numerically as a function of the division level and the target accuracy. These values are also tabulated in the paper.

Often, instead of using the accurately computed values for L, approximation based on the excess band-width formula [6] is used,

$$L = kd + 1.8q^{2/3}(kd)^{1/3}, \tag{97}$$

where $d = k\sqrt{3}a_l$. Comparing these values with the values given in [P6] one can see that the approximated values are often inaccurate, particularly yielding too low estimates for L for lower levels. An improved approximation has been given by Hastriter et al. [26].

6 Summary of the Articles

[P1]: Perfectly Anisotropic Impedance Boundary

In [P1], the class of perfectly anisotropic boundaries (PABs) is defined and some of its scattering properties are studied. The surface impedance and admittance dyadics can be characterized as two-dimensional dyadics, and thus they can be expanded in terms of four basis dyadics. The basis dyadics are either isotropic or anisotropic, and so a surface admittance or impedance dyadic is also either isotropic or anisotropic depending on the basis dyadics that define them. A PAB surface admittance or impedance has as components only basis dyadics that are anisotropic.

A method of realization for a planar PAB is found based on a layer of waveguiding anisotropic material backed by a PEC plane and an expression for the PAB impedance dyadic as a function of the material parameters is derived.

Also, the reflection properties of the PAB are studied, and it is found that a PAB can act as a polarization transformer, e.g. it can transform

a linearly polarized incident field into an elliptically polarized one and vice versa. This property can be further applied to transform an elliptic polarization to another elliptic polarization through reflections upon two PAB planes.

[P2]: Realization of Generalized Soft-and-Hard Boundary

Generalized Soft-and-Hard Surface (GSHS) boundary has been previously defined in [44]. In [P2], a possible realization for such surfaces is proposed and their reflection properties, especially regarding polarization transforming, are studied. As in [P1], a slab of special wave-guiding anisotropic material backed by a PEC plate is used for the realization. Analytic expressions for the material parameters and the surface admittance are derived, and it is verified that they satisfy the GSHS boundary conditions. With these analytic expressions, it is in theory possible to implement any GSHS boundary.

As the class of GSHS boundaries covers a large scale of possible boundaries, also the polarization transforming properties of such structures are diverse. The GSHS boundary is shown to be able to transform any polarization, be it linear, circular, or elliptic, to another for incident waves arriving from the normal direction. The choice of parameters defining the GSHS boundary condition and the corresponding material parameters and their effect to the polarization transforming properties have been studied in detail.

[P3]: Singularity Subtraction Integral Formulae for Surface Integral Equations with RWG, Rooftop, and Hybrid Basis Functions

The main results of the paper [P3] are the singularity subtraction formulae for the numerical integration of surface integral equations with $\hat{\boldsymbol{n}}\times$RWG, rooftop, and $\hat{\boldsymbol{n}}\times$rooftop functions ($\hat{\boldsymbol{n}} \times \boldsymbol{f}$ notation means that the current flow inside the basis function has been rotated by 90°). Previously, the singularity subtraction formulae for RWG functions had been widely published in the literature, but their presentation had been somewhat fragmented and difficult to assemble coherently [4, 13, 22, 83]. In [P3] a comprehensive collection of these singularity subtraction formulae are derived for the rooftop and the RWG functions in a uniform way.

Although RWG functions are, justifiably, widely used in electromagnetic computations, there are situations where the rooftop functions are more suitable. These situations often involve anisotropic surfaces, e.g. as discussed in the papers [P4] and [P5].

The formulae given in [P3] are numerically verified to give accurate results, by using Duffy's transformation and a straight-forward Gaussian quadratures to compare the results. The singularity subtraction formulae give considerably more accurate results with a smaller number of integration points than the other methods. Also, in some situations, the other methods failed to achieve as good accuracies even with a very high number of integration points.

[P4]: Method of Moments Analysis of the Backscattering Properties of a Corrugated Trihedral Corner Reflector

In [P4] a new numerical method to analyze electromagnetic scattering from Soft-and-Hard Surfaces by using a surface integral equation method with Method of Moments is introduced. The application considered in [P4] is a corrugated trihedral corner reflector, which has some interesting applications in radar technology and remote sensing.

The numerical method assumes that the corrugated surface is ideally tuned to the incident wavelength, i.e. it models the SHS perfectly. In the numerical simulations, a novel method to model the SHS by an appropriate choice and configuration of the basis functions is introduced. Similarly, an integral equation formulation that is suited for the SHSs is derived.

The backscattered fields from the trihedral corner reflector are computed for different combinations of PEC and SHS plates covering the inside faces of the reflector, and for various incident fields. The results are verified by Physical Optics (PO) method. The scattering properties of the trihedral corner reflector had been previously studied with less complex methods, e.g. analytically using reflection dyadics and numerically using PO, but a rigorous numerical study of the scattering from such a structure had not been made. In the above mentioned studies, some interesting scattering properties were found, and these results were duplicated by the numerical analysis in [P4].

[P5]: Implementation of Method of Moments for Numerical Analysis of Corrugated Surfaces with Impedance Boundary Condition

The paper [P5] is a continuation of the research presented in the paper [P4]. In [P4] it was assumed that the corrugated surface is ideally tuned to the incident wavelength, so that it can be assumed to be an ideal model for an SHS. In [P5] this condition is relaxed a bit by allowing the depth and the width of the corrugation to diverge slightly from the ideal values.

To be able to numerically compute the scattering fields from such a 'non-ideal' surface, the impedance boundary condition (IBC) must be used.

The main result of paper [P5] is the introduction of an IBC based integral equation formulation to model anisotropic impedance surface that closely resemble the SHS surface. By using Method of Moments (MoM), the scattered fields for various different corrugation types and incident fields are computed. The results are verified by a commercial field computation program *CST Microwave Studio*. The computational results are found to agree well with each other. The limitations of the IBC approximation of the corrugation are found and given in the paper.

Although the corrugation is the main application considered for the IBC integral equation formulation, the method can also be used for other anisotropic impedance boundaries, provided that they fall within the applicable limits of the method that are given in the paper.

[P6]: Efficient Evaluation of the Rokhlin Translator in Multilevel Fast Multipole Algorithm

In [P6], a fast and efficient Fast Fourier Transform (FFT) based oversampling method for interpolating the values of the Rokhlin translator is proposed. This oversampling method allows the use of much smaller initial sampling rate, thus minimizing the memory usage, and the method also leads to a smaller number of points in the interpolation stencil which makes the interpolation much faster than before.

By treating the Rokhlin translator as a trigonometric polynomial, the original sampling rate can be minimized, as the sampling must only be done at the Nyquist rate. Since oversampling by FFT is very fast, it is possible to increase the sampling rate with a very low cost. This in turn allows the use of a smaller number of stencil points for the Lagrange interpolation, which further minimizes the computational cost.

The interpolation parameters, i.e. the oversampling factor s and the number of stencil points $2p$, are optimized with respect to the relative error in the translated (incoming) field. Previously, only the relative error of the interpolation has been used in the optimizations. However, using the field error more realistic values for the interpolation parameters can be achieved.

Two different methods are used to optimize the interpolation parameters. First, the optimal parameter pairs are found by an extensive numerical search. After that, an analytic upper bound is used to compute the optimal pairs. The computed (p, s) pairs are tabulated in the article for a range of division levels and the relative target field accuracies, and can be

used to obtain optimal accuracy and maximal speed-up and memory savings in practical computations. Also, the accurate orders L of the Rokhlin translator as a function of the division level and the target accuracy are tabulated.

References

[1] J.-P. Berenger. 1994. A perfectly matched layer for the absorption of electromagnetic waves. Journal of Computational Physics 114, pages 185–200.

[2] J. Board and K. Schulten. 2000. The fast multipole algorithm. Computing in Science & Engineering 2, no. 1, pages 76–79.

[3] A. Bondeson, T. Rylander, and P. Ingelström. 2005. Computational Electromagnetics. Springer.

[4] S. Caorsi, D. Moreno, and F. Sidoti. 1993. Theoretical and numerical treatment of surface integrals involving the free-space Green's function. IEEE Transactions on Antennas and Propagation 41, no. 9, pages 1296–1301.

[5] W. C. Chew, V. Jandyala, C.C. Lu, E. Michielssen, B Shanker, J. M. Song, and J.S. Zhao. 1997. Fast multilevel techniques for solving integral equations in electromagnetics. In: Asia Pacific Microwave Conference, pages 457–460.

[6] W. C. Chew, J.-M. Jin, E. Michielssen, and J. Song (editors). 2001. Fast and Efficient Algorithms in Computational Electromagnetics. Artech House.

[7] R. Coifman, V. Rokhlin, and S. Wandzure. 1993. The fast multipole method for the wave equation: a pedestrian prescription. IEEE Antennas and Propagation Magazine 35, no. 3, pages 7–12.

[8] R. E. Collin. 1991. Field Theory of Guided Waves. IEEE Press, second edition.

[9] D. Colton and R. Kress. 1983. Integral Equation Methods in Scattering Theory. Wiley.

[10] D. Colton and R. Kress. 1992. Inverse Acoustic and Electromagnetic Scattering Theory, volume 93 of *Applied Mathematical Sciences*. Springer-Verlag.

[11] J. Dongarra and F. Sullivan. 2000. Guest editors introduction to the top 10 algorithms. Computing in Science & Engineering 2, no. 1, pages 22–23.

[12] M. G. Duffy. 1982. Quadrature over a pyramid or cube of integrands with a singularity at a vertex. SIAM Journal on Numerical Analysis 19, pages 1260–1262.

[13] T. F. Eibert and V. Hansen. 1995. On the calculation of potential integrals for linear source distributions on triangular domains. IEEE Transactions on Antennas and Propagation 43, no. 12, pages 1499–1502.

[14] N. Engheta, W. D. Murphy, V. Rokhlin, and M. S. Vassiliou. 1992. The fast multipole method (FMM) for electromagnetic scattering problems. IEEE Transactions on Antennas and Propagation 40, no. 6, pages 634–641.

[15] M. A. Epton and B. Dembart. 1995. Multipole translation theory for the three-dimensional Laplace and Helmholtz equations. SIAM Journal on Scientific Computing 16, no. 4, pages 865–897.

[16] Ö. Ergül and L. Gürel. 2006. Enhancing the accuracy of interpolations and anterpolations in MLFMA. IEEE Antennas and Wireless Propagation Letters 5, pages 467–470.

[17] Ö. Ergül and L. Gürel. 2006. Optimal interpolation of translation operator in multilevel fast multipole algorithm. IEEE Transactions on Antennas and Propagation 54, no. 12, pages 3822–3826.

[18] Ö. Ergül and L. Gürel. 2007. Linear-linear basis functions for MLFMA solutions of magnetic-field and combined-field integral equations. IEEE Transactions on Antennas and Propagation 55, no. 4, pages 1103–1110.

[19] I. A. Eshrah and A. A. Kishk. 2007. Electric-type Green's functions for a corrugated rectangular metaguide based on asymptotic boundary conditions. IEEE Transactions on Antennas and Propagation 55, no. 2, pages 355–363.

[20] C. Gennarelli, G. Pelosi, and G. Riccio. 1998. Physical optics analysis of the field backscattered by a depolarising trihedral corner r<meflector. IEE Proceedings Microwaves, Antennas and Propagation 145, no. 3, pages 213–218.

[21] A. W. Glisson, M. Orman, F. Falco, and D. Koppel. 1995. Electromagnetic scattering by an arbitrarily shaped surface with an anisotropic impedance boundary condition. ACES Journal 10, no. 3, pages 93–106.

[22] R. D. Graglia. 1993. On the numerical Integration of the linear shape functions times the 3-D Green's function or its gradient on a plane triangle. IEEE Transactions on Antennas and Propagation 41, no. 10, pages 1448–1455.

[23] L. Greengard and V. Rokhlin. 1987. A fast algorithm for particle simulations. Journal of Computational Physics , no. 135, pages 280–292.

[24] L. Gürel and Ö. Ergül. 2007. Fast and accurate solutions of extremely large integral-equation problems discretised with tens of millions of unknowns. IEE Electronics Letters 43, no. 9, pages 499–500.

[25] R. F. Harrington. 1993. Field Computation by Moment Methods. IEEE Press.

[26] M. L. Hastriter, S. Ohnuki, and W. C. Chew. 2003. Error control of the translation operator in 3D MLFMA. Microwave and Optical Technology Letters 37, no. 3, pages 184–188.

[27] D. J. Hoppe and Y. Rahmat-Samii. 1995. Impedance Boundary Conditions in Electromagnetics. Taylor & Francis.

[28] S. Järvenpää, M. Taskinen, and P. Ylä-Oijala. 2003. Singularity extraction technique for integral equation methods with higher order basis functions on plane triangles and tetrahedra. International Journal for Numerical Methods in Engineering 58, pages 1149–1165.

[29] S. Järvenpää, M. Taskinen, and P. Ylä-Oijala. 2006. Singularity subtraction technique for high-order polynomial vector basis functions on planar triangles. IEEE Transactions on Antennas and Propagation 54, no. 1, pages 42–49.

[30] J. Jin. 2002. The Finite Element Method in Electromagnetics. Wiley, 2nd edition.

[31] R. C. Booton Jr. 1992. Computational Methods for Electromagnetics and Microwaves. Wiley.

[32] M. A. Khayat and D. R. Wilton. 2005. Numerical evaluation of singular and near-singular potential integrals. IEEE Transactions on Antennas and Propagation 53, no. 10, pages 3180–3190.

[33] P.-S. Kildal. 1988. Definition of artificially soft and hard surfaces for electromagnetic waves. IEE Electronics Letters 24, no. 3, pages 168–170.

[34] P.-S. Kildal. 1990. Artificially soft and hard Surfaces in electromagnetics. IEEE Transactions on Antennas and Propagation 38, no. 10, pages 1537–1544.

[35] P.-S. Kildal. 2000. Foundations of Antennas, A Unified Approach. Studentlitteratur.

[36] A. A. Kishk. 2003. Analysis of hard surfaces of cylindrical structures of arbitrarily shaped cross section using asymptotic boundary conditions. IEEE Transactions on Antennas and Propagation 51, no. 6, pages 1150–1156.

[37] A. A. Kishk. 2004. Electromagnetic scattering from transversely corrugated cylindrical structures using the asymptotic corrugated boundary conditions. IEEE Transactions on Antennas and Propagation 52, no. 11, pages 3104–3108.

[38] A. A. Kishk and P.-S. Kildal. 1995. Electromagnetic scattering from two dimensional anisotropic impedance object under oblique plane wave incidence. ACES Journal 10, no. 3, pages 81–92.

[39] A. A. Kishk, P. Slättman, and P.-S. Kildal. 1999. Radiation from 3D sources in the presence of 2D composite objects of arbitrary cross-sectional shape. ACES Journal 14, no. 1, pages 17–24.

[40] S. Koc, J. Song, and W. C. Chew. 1999. Error analysis for the numerical evaluation of the diagonal forms of the scalar spherical addition theorem. SIAM Journal on Numerical Analysis 36, no. 3, pages 906–921.

[41] B. M. Kolundzija and A. R. Djordjević. 2002. Electromagnetic Modeling of Composite Metallic and Dielectric Structures. Artech House.

[42] K. S. Kunz and R. J. Luebbers. 1993. The Finite Difference Time Domain Method for Electromagnetics. CRC Press.

[43] I. V. Lindell. 1992. Methods for Electromagnetic Field Analysis. Engineering Science. Oxford University Press.

[44] I. V. Lindell. 2002. Generalized soft-and-hard surface. IEEE Transactions on Antennas and Propagation 50, no. 7, pages 926–929.

[45] I. V. Lindell and P. P. Puska. 1996. Reflection dyadic for the soft and hard surface with application to the depolarising corner reflector. IEE Proceedings Microwaves, Antennas and Propagation 143, no. 5, pages 417–421.

[46] I. V. Lindell and A. H. Sihvola. 2005. Perfect electromagnetic conductor. Journal of Electromagnetic Waves and Applications 19, no. 7, pages 861–869.

[47] I. V. Lindell and A. H. Sihvola. 2005. Realization of the PEMC boundary. IEEE Transactions on Antennas and Propagation 53, no. 9, pages 3012–3018.

[48] I. V. Lindell and A. H. Sihvola. 2006. Realization of impedance boundary. IEEE Transactions on Antennas and Propagation 54, no. 12, pages 3669–3676.

[49] A. Macikunas and S. Haykin. 1993. Trihedral twist-grid polarimetric reflector. IEE Proceedings F 140, no. 4, pages 216–222.

[50] D. G. Michelson and E. V. Jull. 1995. Depolarizing trihedral corner reflectors for radar navigation and remote sensing. IEEE Transactions on Antennas and Propagation 43, no. 5, pages 513–518.

[51] E. K. Miller, L. Medgyesi-Mitschang, and E. H. Newman (editors). 1992. Computational Electromagnetics, Frequency-Domain Method of Moments. IEEE Press.

[52] P. Monk. 2003. Finite Element Methods for Maxwell's Equations. Oxford University Press.

[53] A. F. Peterson, S. L. Ray, and R. Mittra. 1998. Computational Methods for Electromagnetics. IEEE Press.

[54] S. M. Rao, D. R. Wilton, and A. W. Glisson. 1982. Electromagnetic scattering by surfaces of arbitrary shape. IEEE Transactions on Antennas and Propagation AP-30, no. 3, pages 409–418.

[55] V. Rokhlin. 1990. Rapid solution of integral equations of scattering theory in two dimensions. Journal of Computational Physics 36, no. 2, pages 414–439.

[56] V. Rokhlin. 1993. Diagonal forms of translation operators for the Helmholtz equation in three dimensions. Applied And Computational Harmonic Analysis 1, no. 82-93.

[57] M. N. O. Sadiku. 1992. Numerical Techniques in Electromagnetics. CRC Press.

[58] M. Salazar-Palma, T. K. Sarkar, L.-E. Carcía-Costillo, T. Roy, and A. Djordjević. 1998. Iterative and Self-Adaptive Finite-Elements in Electromagnetic Modeling. Artech House.

[59] J. Sarvas. 2003. Performing inteprolation and anterpolation entirely by fast fourier transform in the 3-D multilevel fast multipole algorithm. SIAM Journal on Numerical Analysis 41, no. 6, pages 2180–2196.

[60] T. B. A. Senior and J. L. Volakis. 1995. Approximate boundary conditions in electromagnetics, volume 41 of *Electromagnetic Waves*. The Institution of Electrical Engineers.

[61] A. Serdyukov, I. Semchenko, S. Tretyakov, and A. Sihvola. 2001. Electromagnetics of Bi-anisotropic Materials, Theory and Applications, volume 11 of *Electrocomponent Science Monographs*. Gordon and Breach Science Publishers.

[62] D. R. Sheen, E. L. Johansen, and L. P. Elenbogen. 1992. The gridded trihedral: a new polarimetric SAR calibration reflector. IEEE Transactions on Geoscience and Remote Sensing 30, no. 6, pages 1149–1153.

[63] P. P. Silvester and G. Pelosi (editors). 1994. Finite Elements for Wave Electromagnetics, Methods and Techniques. IEEE Press.

[64] Z. Sipus, H. Merkel, and P.-S. Kildal. 1997. Green's functions for planar soft and hard surfaces derived by asymptotic boundary conditions. IEE Proceedings Microwaves, Antennas and Propagation 144, no. 5, pages 321–328.

[65] J. Song and W. C. Chew. 2001. Interpolation of translation matrix in MLFMA. Microwave and Optical Technology Letters 30, no. 2, pages 109–114.

[66] J. Song, C.-C. Lu, and W. C. Chew. 1997. Multilevel fast multipole algorithm for electromagnetic scattering by large complex objects. IEEE Transactions on Antennas and Propagation 45, no. 10, pages 1488–1493.

[67] J. M. Song and W. C. Chew. 1995. Multilevel fast-multipole algorithm for solving combined field integral equations of electromagnetic scattering. Microwave and Optical Technology Letters 10, no. 1, pages 14–19.

[68] C. W. Steele (editor). 1987. Numerical Computation of Electric and Magnetic Fields. Van Nostrand Reinhold Company.

[69] A. Taflove and S. C. Hagness. 2005. Computational Electrodynamics, The Finite-Difference Time-Domain Method. Artech House, 3rd edition.

[70] W.-H. Tang and S. D. Gedney. 2006. An efficient evaluation of near singular surface integrals via the Khayat-Wilton transform. Microwave and Optical Technology Letters 48, no. 8, pages 1583–1586.

[71] D. J. Taylor. 2003. Accurate and efficient numerical integration of weakly singular integrals in Galerkin EFIE solutions. IEEE Transactions on Antennas and Propagation 51, no. 7, pages 1630–1637.

[72] M. S. Tong and W. C. Chew. 2007. Super-hyper singularity treatment for solving 3D electric field integral equations. Microwave and Optical Technology Letters 49, no. 6, pages 1383–1388.

[73] S. A. Tretyakov. 2003. Analytical modeling in applied electromagnetics. Artech House.

[74] T. M. Uusitupa. 2006. Usability studies on approximate corrugation models in scattering analysis. IEEE Transactions on Antennas and Propagation 54, no. 9, pages 2486–2496.

[75] S. Velamparambil, W. C. Chew, and J. Song. 2003. 10 million unknowns: is it that big? IEEE Antennas Propag. Mag. 45, no. 2, pages 43–58.

[76] J. L. Volakis, A. Chatterjee, and L. C. Kempel. 1998. Finite Element Method for Electromagnetics. IEEE Press.

[77] H. Wallén, S. Järvenpää, P. Ylä-Oijala, and J. Sarvas. 2007. Broadband Müller-MLFMA for electromagnetic scattering by dielectric objects. IEEE Transactions on Antennas and Propagation 55, no. 5, pages 1423–1430.

[78] H. Wallén and J. Sarvas. 2005. Translation procedures for broadband MLFMA. Progress In Electromagnetics Research 55, pages 47–78.

[79] J. J. H. Wang. 1991. Generalized Moment Methods in Electromagnetics. Wiley.

[80] D. R. Wilton, S. M. Rao, A. W. Glisson, D. H. Schaubert, O. M. Al-Bundak, and C. M. Butler. 1984. Potential integrals for uniform and linear source distributions on polygonal and polyhedral domains. IEEE Transactions on Antennas and Propagation AP-32, no. 3, pages 276–281.

[81] K. S. Yee. 1966. Numerical solution of initial boundary values involving Maxwell's equations in isotropic media. IEEE Transactions on Antennas and Propagation 14, pages 302–307.

[82] Z. Ying, P.-S. Kildal, and A. A. Kishk. 1996. Study of different realizations and calculation models for soft surfaces by using a vertical monopole on a soft disk as a test bed. IEEE Transactions on Antennas and Propagation 44, no. 11, pages 1474–1481.

[83] P. Ylä-Oijala and M. Taskinen. 2003. Calculation of CFIE impedance matrix elements with RWG and $n\times$ RWG functions. IEEE Transactions on Antennas and Propagation 51, no. 8, pages 1837–1846.

1. L. Jylhä: Modeling of electrical properties of composites, March 2008.

2. I. Torniainen: Multifrequency studies of gigahertz-peaked spectrum sources and candidates, May 2008.

3. I. Hänninen: Analysis of electromagnetic scattering from anisotropic impedance boundaries, June 2008.

ISBN 978-951-22-9400-8 (printed)
ISBN 978-951-22-9401-5 (electronic)
http://lib.tkk.fi/Diss/2008/isbn9789512294015/
ISSN 1797-4364
Picaset Oy, Helsinki 2008